

Chemical abundances of solar neighborhood RR Lyrae stars[★]

E. Pancino^{1,2†}, N. Britavskiy^{3,4,5}, D. Romano¹, C. Cacciari¹, A. Mucciarelli⁵,
and G. Clementini¹

¹INAF-Osservatorio Astronomico di Bologna, Via Ranzani 1, I-40127 Bologna, Italy

²ASI Science Data Center, Via del Politecnico snc, I-00133 Roma, Italy

³IAASARS, National Observatory of Athens, GR-15236 Penteli, Greece

⁴Department of Astronomy and Astronomical Observatory, Odessa National University, T.G. Shevchenko Park, Odessa, 65014, Ukraine

⁵Dipartimento di Fisica e Astronomia, Università di Bologna, Viale Berti Pichat 6/2, I-40127 Bologna, Italy

Accepted ... Received ...; in original form ...

ABSTRACT

We have analysed a sample of 18 RR Lyrae stars (17 fundamental-mode — RRAb — and one first overtone — RRC) and three Population II Cepheids (two BL Her stars and one W Vir star), for which high-resolution ($R \geq 30\,000$), high signal-to-noise ($S/N \geq 30$) spectra were obtained with either SARG at the Telescopio Nazionale Galileo (La Palma, Spain) or UVES at the ESO Very Large Telescope (Paranal, Chile). Archival data were also analyzed for a few stars, sampling ≥ 3 phases for each star. We obtained atmospheric parameters (T_{eff} , $\log g$, v_t , and $[M/H]$) and abundances of several iron-peak and α -elements (Fe, Cr, Ni, Mg, Ca, Si, and Ti) for different pulsational phases, obtaining $\langle [\alpha/\text{Fe}] \rangle = +0.31 \pm 0.19$ dex over the entire sample covering $-2.2 < [\text{Fe}/H] < -1.1$ dex. We find that silicon is indeed extremely sensitive to the phase, as reported by previous authors, and cannot be reliably determined. Apart from this, metallicities and abundance ratios are consistently determined, regardless of the phase, within 0.10–0.15 dex, although caution should be used in the range $0 \leq \phi \leq 0.15$. Our results agree with literature determinations for both variable and non-variable field stars, obtained with very different methods, including low and high-resolution spectroscopy. W Vir and BL Her stars, at least in the sampled phases, appear indistinguishable from RRAb from the spectroscopic analysis point of view. Our large sample, covering all pulsation phases, confirms that chemical abundances can be obtained for RR Lyrae with the classical EW-based technique and static model atmospheres, even rather close to the shock phases.

Key words: stars: abundances – stars: variables: general – stars: variables: RR Lyrae – stars: variables: Cepheids.

1 INTRODUCTION

RR Lyrae stars are old, metal-poor, horizontal branch pulsating variables that are undergoing quiescent helium burning in their centres. With typical periods of 0.2–1.0 day and magnitude variations in the visual band of 0.3–1.6 mag, they are called RRAb, RRC or RRd (Bailey 1902; Jerzykiewicz & Wenzel 1977), respectively, depending on whether they are pulsating in the radial fundamental mode, radial first overtone, or both modes simultaneously. Once appropriate corrections are made for evolutionary effects and for the fact that the mean intrinsic absolute magnitudes are not constant (actually, they correlate with metallicity: Cacciari & Clementini

2003, and references therein), RR Lyrae turn out to be excellent distance indicators, probing stellar populations in the Milky Way and beyond: RRAb stars are routinely used to trace tidal tails and streams in the Galactic halo, with important advantages compared to main-sequence turnoff stars, blue horizontal branch stars and K giants (e.g. Vivas et al. 2008; Sesar et al. 2010, 2013; Drake et al. 2013) and to probe the structure of external systems (e.g. Moretti et al. 2014). Several nearby RR Lyrae and variable stars do indeed have parallaxes in the literature, either from Hipparcos (Høg et al. 2000; van Leeuwen 2007) or from dedicated studies (Benedict et al. 2011). In the near future, the Gaia¹ ESA mission will provide parallaxes to the μas level for all nearby stars. Photometry, which has been traditionally used for RR Lyrae distance determination, needs to be complemented by spectroscopic information not only to account correctly for the effect of metallicity on the ab-

[★] Based on data collected with UVES@VLT under program ID 083.B-0281 and with SARG@TNG under program IDs AOT 19 TAC 11 and AOT 20 TAC 83. Also based on ESO FEROS and HARPS archival reduced data products, under program IDs 079.D-0462 and 178.D-0361.
[†] email:elena.pancino@oabo.inaf.it

¹ <http://www.cosmos.esa.int/web/gaia>

Table 1. Basic information for the programme stars.

Star	R.A.(J2000) (h m s)	Decl.(J2000) (° ' ")	Type	alt (Type)	V (mag)	Epoch (JD 2400000+)	Period (day)	A(V) (mag)	[Fe/H] _{K06} (dex)	[Fe/H] _{B00} (dex)
DR And*	01 05 10.71	+34 13 06.3	RRab	(W Uma)	11.65 – 12.94	51453.158583	0.5631300	1.10	-1.42±0.20	-1.48
X Ari	03 08 30.88	+10 26 45.2	RRab		11.28 – 12.60	54107.2779	0.6511681	0.88	-2.08±0.17	-2.43
TW Boo	14 45 05.94	+41 01 44.1	RRab		10.63 – 11.68	53918.4570	0.53226977	1.06	-1.53±0.16	-1.46
TW Cap	20 14 28.42	-13 50 07.9	CWa		9.95 – 11.28	51450.139016	28.610100	(0.84)	—	-1.20
RX Cet	00 33 38.28	-15 29 14.9	RRab		11.01 – 11.75	52172.1923	0.5736856	0.60	-1.09±0.32	-1.28
U Com	12 40 03.20	+27 29 56.1	RRc		11.50 – 11.97	51608.348633	0.2927382	(0.34)	—	-1.25
UZ CVn	12 30 27.70	+40 30 31.9	RRab		11.30 – 12.00	51549.365683	0.6977829	1.03	-2.10±0.17	-1.89
AE Dra	18 27 06.63	+55 29 32.8	RRab		12.40 – 13.38	51336.369463	0.6026728	1.16	-1.88±0.17	-1.54
BK Eri	02 49 55.88	-01 25 12.9	RRab		12.00 – 13.05	51462.198773	0.5481494	0.86	—	-1.64
UY Eri	03 13 39.13	-10 26 32.4	CWb		10.93 – 11.66	51497.232193	2.2132350	(0.64)	—	-1.60
SZ Gem	07 53 43.45	+19 16 23.9	RRab		10.98 – 12.25	51600.336523	0.5011365	1.27	-1.67±0.16	-1.46
VX Her	16 30 40.80	+18 22 00.6	RRab		9.89 – 11.21	53919.451	0.45536088	1.27	-1.40±0.16	-1.58
DH Hya*	09 00 14.83	-09 46 44.1	RRab	(W Uma)	11.36 – 12.65	51526.426583	0.4889982	1.28	-1.73±0.16	-1.55
V Ind	21 11 29.91	-45 04 28.4	RRab		9.12 – 10.48	47812.668	0.479601	(1.06)	—	-1.50
SS Leo	11 33 54.50	-00 02 00.0	RRab		10.38 – 11.56	53050.565	0.626335	1.06	-1.93±0.17	-1.79
V716 Oph	16 30 49.47	-05 30 19.5	CWb		8.97 – 9.95	51306.272953	1.1159157	(1.39)	—	-1.55
VW Scl	01 18 14.97	-39 12 44.9	RRab		10.40 – 11.40	27809.381	0.5109147	(1.23)	—	-0.84
BK Tuc	23 29 33.33	-72 32 40.0	RRab		12.40 – 13.30	36735.605	0.5502000	(0.94)	—	-1.82
TU UMa	11 29 48.49	+30 04 02.4	RRab		9.26 – 10.24	51629.148846	0.5576587	0.96	-1.66±0.17	-1.51
RV UMa	13 33 18.09	+53 59 14.6	RRab		9.81 – 11.30	51335.380433	0.4680600	1.07	-1.20±0.18	-1.20
UV Vir	12 21 16.74	+00 22 03.0	RRab		11.35 – 12.35	51579.459853	0.5870824	1.00	-1.73±0.18	-1.19

Notes. Coordinates (columns 2 and 3), type of variability (columns 4 and 5), rough magnitude ranges (column 6), and adopted periods (column 8) are from the General Catalog of Variable Stars (GCVS, Samus et al. 2010), except for X Ari, TW Boo, RX Cet, and VX Her, that are known to have a variable period (Le Borgne et al. 2007, see also text). Stars marked with an asterisk do not have a clear classification, but for our computations we used the type in column 4. Epochs of maximum light (column 7) have been derived by us from ROTSE light curves, except for X Ari, TW Boo, RX Cet, and VX Her, where a parabolic fit was used, based on data from Le Borgne et al. (2007). For a few stars with no ROTSE data, epochs are taken from the GCVS, and for SS Leo from Maintz (2005). *V* amplitudes (column 9) are from Kinemuchi et al. (2006); values in brackets were either derived from ROTSE light curves (TW Cap, U Com, UY Eri, and V716 Oph), or taken from the ASAS-3 catalogue (V Ind, VW Scl, BK Tuc; Pojmanski 1997; Meyer 2006). Metallicities are from Kinemuchi et al. (2006, column 10) and Beers et al. (2000, column 11; typical errors are on the order 0.1–0.2 dex).

solute magnitude of these stars, but also to give information on their kinematics and detailed chemical abundances (whenever possible) which both help discriminate among various sub-populations with different characteristics.

However, while extensive literature exists concerning photometry and low-resolution spectroscopy of RR Lyrae stars, high-resolution spectroscopic studies are by far less numerous. This is most likely due to the limits on the exposure times, which translate into limits on the attainable S/N (signal-to-noise) ratios in the spectra, imposed by the short pulsation periods. Yet, a number of authors (Butler et al. 1976, 1979; Clementini et al. 1995; Lambert et al. 1996; Preston et al. 2006; Kolenberg et al. 2010; For et al. 2011; Kinman et al. 2012; Govea et al. 2014) did perform detailed chemical composition analyses based on high-resolution spectra for different samples of RR Lyrae stars. The most important general conclusions that can be drawn from these studies are: (i) lines of most species form in local thermal equilibrium (LTE) conditions, thus standard LTE analyses can be performed, but see our discussions in Sections 4.2 and 4.4 for more details; (ii) co-addition of spectra can be safely used to increase the S/N ratios; (iii) the strongest and more symmetric lines are found at phases $0.3 < \phi < 0.5$; (iv) effective temperature (T_{eff}), gravity ($\log g$), and microturbulent velocity (v_t) variations with phase are regular, but abundance ratios are mostly insensitive to phase.

High-resolution spectroscopic studies are mandatory in order to gain insights on the atmospheric behaviour of RR Lyrae stars. Our knowledge of the atmospheric dynamics in RR Lyrae stars is, in fact, still very poor. For instance, the physical origin of the

Blazhko effect – so named after Sergei Nikolaevich Blazhko, who was the first to report a long-period modulation of the lightcurve of a RR Lyrae star (Blazhko 1907) – remains frustratingly elusive (e.g. Chadid et al. 2008; Chadid & Preston 2013, and references therein), in spite of the fact that a significant fraction of RRab stars (up to 50 per cent; Jurcsik et al. 2009) exhibits these long-term modulations of amplitudes and phases. We refer the interested reader to Fossati et al. (2014) for the most recent high-resolution spectroscopic study of RR Lyr, dealing with all the above issues.

Population II Cepheids also play a relevant role as distance indicators and old stellar populations tracers. They are generally classified as BL Her, W Vir and RV Tau according to their periods and evolutionary stages: BL Her stars have the shortest periods (0.8–4 days) and are evolving from the horizontal branch towards the asymptotic giant branch (AGB); W Vir stars, with periods in the range 4–20 days, are crossing the instability strip during their blue-loop excursions; and RV Tau stars are in their post-AGB phase (see e.g. Soszyński et al. 2008). Despite some hints of unusual chemical compositions, they have received scant attention from spectroscopists. A notable exception is the study by Maas et al. (2007), who analysed a sample of 19 BL Her and W Vir stars and related the contrasting abundance anomalies to the different stars' evolutionary stages from the blue horizontal branch. Two of the three Population II Cepheids in our sample have abundance determinations from Maas et al. (2007): TW Cap and UY Eri.

In this paper, we present atmospheric parameters, metallicities, and abundances of several iron-peak and α -elements for 18 RR Lyrae stars and 3 Population II Cepheids, observed at differ-

Table 2. Observing logs.

Star	Inst.	Exp _n	Observation date (HJD 2400000+)	Phase	t _{exp} (min)	S/N	Star	Inst.	Exp _n	Observation date (HJD 2400000+)	Phase	t _{exp} (min)	S/N
DR And	SARG	1	55084.57606	0.63	30	80	V Ind	FEROS	1*	54302.85087	0.46	12	80
	SARG	2	55084.60982	0.69	60	80		FEROS	2*	54302.92066	0.61	15	70
	SARG	3	55111.42640	0.31	60	80		FEROS	3*	54302.93328	0.63	20	70
X Ari	APO	1*	55521.74265	0.19	20	140		HARPS	1*	54303.90886	0.67	20	30
TW Boo	SARG	1	54921.57757	0.61	30	70		HARPS	2*	54303.91963	0.69	20	30
	SARG	2	54921.59904	0.65	30	70		HARPS	3*	54303.93260	0.71	20	30
	SARG	3	54921.62052	0.69	30	70		HARPS	4*	54304.72958	0.38	20	30
TW Cap	UVES	1	55070.65106	0.54	8	160		HARPS	5*	54304.74426	0.41	20	30
RX Cet	SARG	1	55107.46135	0.51	45	130		HARPS	6*	54304.90275	0.74	20	20
U Com	SARG	1	54922.40036	0.87	30	60		HARPS	7*	54304.91729	0.77	20	20
	SARG	2	54922.42337	0.95	30	60		HARPS	8*	54304.93168	0.80	20	20
	SARG	3	54922.44483	0.02	30	60		HARPS	9*	54305.90708	0.83	30	20
UZ CVn	SARG	1	54922.47495	0.04	45	70		HARPS	10*	54305.92491	0.87	30	30
	SARG	2	54922.50919	0.08	45	60	SS Leo	UVES	1	54951.53090	0.06	7.5	65
	SARG	3	54922.54108	0.13	45	60		UVES	2	54951.53683	0.07	7.5	85
AE Dra	SARG	1	54921.70407	0.05	30	45	V716 Oph	UVES	1	55081.50566	0.08	30	120
	SARG	2	54921.73314	0.10	45	50	VW Scl	UVES	1*	52168.62787	0.71	3	90
BK Eri	UVES	1*	52169.88146	0.04	7	100		UVES	2*	52167.87013	0.23	3	120
	UVES	2*	52168.87630	0.20	7	80		UVES	3*	52166.89349	0.32	3	90
	UVES	3*	52167.74787	0.14	7	90		UVES	4*	52165.78284	0.15	3	120
	UVES	4*	52166.85011	0.51	7	70		UVES	5*	52166.75294	0.05	3	150
UY Eri	SARG	1	55085.72750	0.38	45	130	BK Tuc	UVES	1	55050.75870	0.17	30	110
SZ Gem	SARG	1	55151.64242	0.50	45	80		UVES	2	55050.80812	0.26	30	80
VX Her	SARG	1	54921.63477	0.86	25	70		UVES	3	55051.84590	0.15	30	70
	SARG	2	54921.66660	0.05	30	70	TU UMa	SARG	1	54922.37438	0.45	30	110
DH Hya	UVES	1	54936.60042	0.79	13	70	RV UMa	SARG	1	54921.47819	0.62	30	60
	SARG	1	54921.40162	0.71	45	35		SARG	2	54921.50074	0.66	30	80
	SARG	2	54921.43822	0.79	45	50		SARG	3	54921.52265	0.71	30	80
V Ind	UVES	1	55026.91751	0.19	4	120	UV Vir	UVES	1	54951.58967	0.87	20	120
	UVES	2	55069.64846	0.29	4	120							

Notes. Archival spectra are marked with an asterisk in columns 3 and 10. The listed S/N are evaluated @6000 Å.

ent phases. The paper is organized as follows. In Section 2 we summarize the observations and data reduction. In Section 3 we describe the adopted model atmospheres, atomic linelist and abundance analysis tool, and present the equivalent width (EW) measurements. Section 4 presents the results of our spectroscopic abundance analysis, starting from the astrophysical parameters determination and ending with the metallicities and abundance ratios of our sample stars. Finally, the results are discussed — and some conclusions are drawn — in Section 5.

2 OBSERVATIONS AND DATA REDUCTION

The observations for the 18 RR Lyrae and 3 Population II Cepheids analysed in this paper have been obtained with two different telescopes and instrumental set-ups and complemented with archive data. Basic literature information for the programme stars can be found in Table 1 (see also Section 2.4).

2.1 SARG data

Observations of 15 RR Lyrae stars (DR And, X Ari, TW Boo, RZ Cam, RX Cet, U Com, RV CrB, SW CVn, UZ CVn, AE Dra,

SZ Gem, VX Her, DH Hya, TU UMa and RV UMa)² and one BL Her star (UY Eri) were carried out with SARG@TNG (Gratton et al. 2001), operated on the island of La Palma, Spain, during two separate runs in March and between September and November 2009. During the first run (in visitor mode), variables were observed almost always at random phases, while in the second run (in service mode) observations were planned at minimum light. The observing conditions in both runs were reasonably good, although non-photometric. Observations were generally split into three exposures (see Table 2); in some cases exposure times as long as 45 or 60 min were necessary to gather enough S/N. This implies that some of these spectra will suffer from significant line smearing, where the distorted profiles from slightly different phases overlap, producing additional distortions in the line shapes. The exact phase and phase coverage of each exposure can be desumed from Table 2 or Figure 1. SARG was set-up to reach a resolving power of $R=\delta\lambda/\lambda \simeq 30\,000$ and to cover a spectral range from 4000 to 8500 Å. The relatively low spectral resolution of SARG does not damage significantly the already widened line profiles of pulsating

² The quality of SARG spectra of RZ Cam, RV CrB, SW CVn, and X Ari was not sufficient to obtain reliable atmospheric parameters and abundances. Therefore, RZ Cam, RV CrB and SW CVn were not analysed, and will not be reported in the following, whereas X Ari was analyzed using archival spectra.

variables. We could reach a S/N roughly between 50 and 100 per pixel except on the margins of the spectra, and we discarded spectra below $S/N \approx 20$ –30, approximately.

SARG spectra were reduced with the IRAF³ tasks in the *echelle* package. First of all we applied bias subtraction and flat-fielding; for preparing flatfields (with *apflatten*) and also for tracing spectra of faint stars we used spectra of the brightest star (one for each night) to locate echelle orders. The position of each order was then traced interactively with a cubic spline. Two-dimensional dispersion solutions were found for the Th-Ar spectra; the typical r.m.s. deviation of the lines from fitted wavelength calibration polynomial was near 0.03 Å. Sky absorption lines (telluric bands of O₂ and H₂O) were removed using the IRAF task *telluric* with the help of our own library of observed spectra of fast rotating hot stars accumulated during the years. In particular, the stars which provided best results in the case of SARG spectra were HR 5206 and HD 6215 observed with UVES in June 2000 at a slightly higher resolution. Once the spectra were wavelength calibrated and extracted (with optimal extraction), the orders were merged into a single spectrum by means of an S/N weighted sum using the IRAF tasks *scombine* and *continuum*. An example of the quality of the SARG spectra is shown in Figure 2.

2.2 UVES data

Eight stars (SW Aqr, TW Cap, DH Hya, V Ind, SS Leo, V716 Oph, BK Tuc and UV Vir)⁴ were observed with UVES@VLT (D’Odorico 2000; Dekker et al. 2000), between April and August 2009 in service mode. Observing conditions were clear, but mostly non-photometric. Being the VLT more efficient, we needed generally shorter exposures than with SARG to reach a similar S/N, resulting in less altered line profiles, covering a shorter range of phases. The observing logs can be found in Table 2 and the phase coverage can be seen in Figure 1. UVES was set-up to reach a resolution of $R \approx 45\,000$ and to cover a spectral range of 4500–7500 Å; the S/N was slightly higher than for SARG spectra, ranging between 70 and 150 per pixel, roughly.

The data reductions were performed with the UVES pipeline (Ballester et al. 2000) by ESO as part of the service observations. The pipeline reductions include the classical steps of bias subtraction, flat-field correction, wavelength calibration and spectra extraction by means of optimal extraction, sky subtraction, and finally order merging with pixel resampling. We normalized the pipeline-processed spectra and corrected them for telluric absorption as done for the SARG spectra.

2.3 Archival data

Additional spectra were retrieved from the ESO Advanced Data Products archive, consisting of extracted and wavelength-calibrated spectra of BK Eri (observed with UVES), V Ind (observed with FEROS and HARPS) and of VW Scl (observed with UVES). A spectrum of X Ari obtained with the ARC Echelle Spectrograph (ARCES) at the Apache Point Observatory (S. Andrievsky, G.

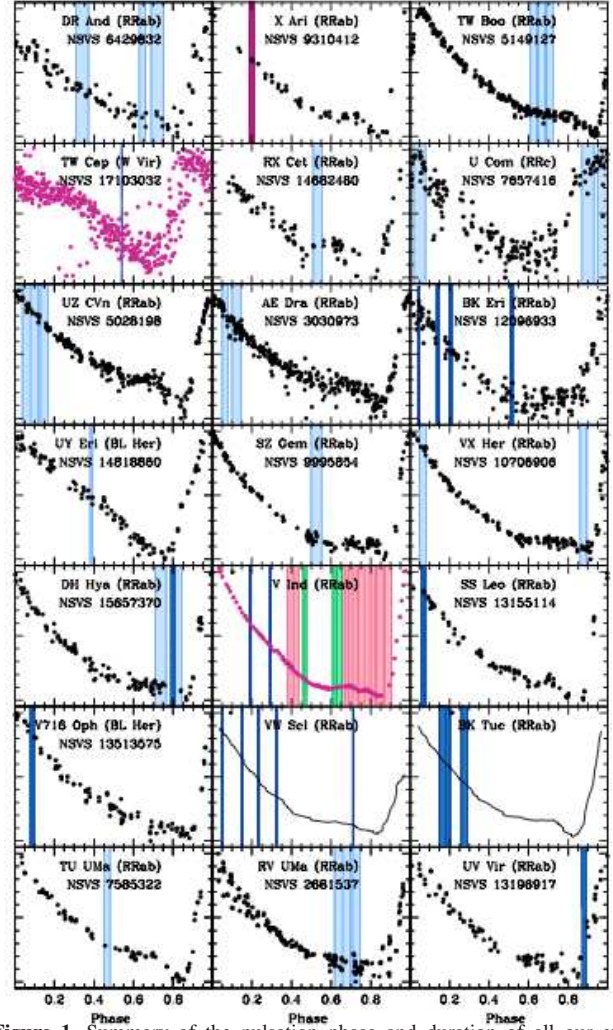


Figure 1. Summary of the pulsation phase and duration of all our exposures: SARG spectra are indicated by light blue stripes; UVES ones by dark blue stripes; archival FEROS spectra by green stripes; archival HARPS spectra by pink stripes; and the APO spectrum of X Ari by a purple stripe. Each panel reports data for one star on an arbitrary scale. Whenever ROTSE light curve data were available, they were plotted as black dots on an arbitrary vertical scale, just for reference, and the ROTSE designation for the star was indicated on each panel. For V Ind, we used data from Clementini, Cacciari, & Lindgren (1990, purple dots); for TW Cap we plotted the ASAS-3 data (Pojmanski 1997; Meyer 2006, purple dots); for VW Scl and BK Tuc we obtained template light curves from data of stars with similar characteristics: SS For (Cacciari et al. 1987) and TU Uma (Liu & Janes 1989; Fernley & Barnes 1997), respectively, plotted as solid curves.

Wallerstein, 2013, private communication) was also included in the sample. Information on these additional spectra can be found in Table 2 and in Figure 1. The spectra were normalised and corrected for telluric absorption features following the procedures adopted for our own SARG and UVES observations.

2.4 Reference literature information

For all our programme candidates, we searched the literature for basic information, which is listed in Tables 1 and 3, and displayed in Figure 1. Epochs of maximum light were derived from ROTSE

³ IRAF (<http://iraf.noao.edu/>) is distributed by the National Optical Astronomical Observatory, which is operated by the Association of Universities for Research in Astronomy (AURA) under cooperative agreement with the National Science Foundation.

⁴ The quality of the spectrum of SW Aqr was not sufficient for an abundance analysis, so SW Aqr will not be reported in the following.

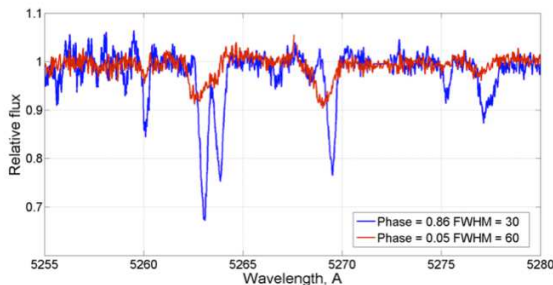


Figure 2. Example of the quality of our SARG spectra. The two spectra of VX Her obtained with SARG are shown. According to Kolenberg et al. (2010) and as described in the text, the $\phi=0.05$ spectrum should correspond to a shocked atmosphere phase, while the $\phi=0.86$ spectrum should correspond to a quiescent phase. The difference between the two spectra is striking (see also figures 7, 8 and 9 of Clementini et al. 1994, for the effect of the shock on the hydrogen and metal lines of RR Lyrae stars in M4).

light curves⁵ (see also Woźniak et al. 2004, for a description of ROTSE variable star observation and analysis) for most of our targets, except for TW Cap, V Ind, VW Scl, and BK Tuc, for which epochs were taken from the General Catalogue of Variable Stars (GCVS, Samus et al. 2010), SS Leo, for which an updated epoch was obtained from Maintz (2005), and for three stars with varying period described below. The periods and the Bailey variability types were obtained from the GCVS. Amplitudes were obtained from Kinemuchi et al. (2006) for most stars, and when these were not available, from ROTSE light curves by us or from the ASAS-3 catalogue (All Sky Automated Survey, Pojmanski 1997). Also, 2MASS photometry and extinction data (see Table 3) were used to derive photometric T_{eff} estimates (Section 4.1). Reference iron abundances were obtained from Beers et al. (2000) and Kinemuchi et al. (2006, see also Sections 4.4 and 4.6).

It is important to note that, according to Fernley et al. (1989), X Ari has varying period. More recently, Le Borgne et al. (2007) found that also TW Boo, RX Cet, and VX Her have variable periods: using their reference data (reported in Table 1) and a parabolic fit (their equation 1), we derived the epoch of maximum light closest to our observations, the appropriate period, and finally the phase of each spectrum (reported in Tables 1 and 2).

3 ABUNDANCE ANALYSIS

Many of our spectra were taken at random phase; Figure 1 summarizes the phase and duration of our exposures: several of our spectra were taken away from optimal phases. We discuss on the implications of using static atmosphere models in Section 3.1, briefly reviewing theoretical and experimental knowledge in the literature. Later (Sections 3.3 and 3.4) we apply the classical method to all our spectra, regardless of their phase. Profiting from the ample phase coverage, we then compare our results of both atmospheric parameters and abundances *a posteriori* (Section 4) across different pulsation phases and with the literature, to assess the reliability and repeatability of our analysis.

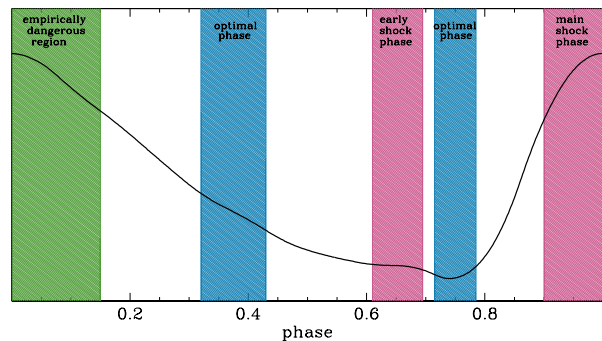


Figure 3. A summary sketch of the quiescent (blue shaded regions) and shock phases (red shaded regions) along the light-curve of a type ab RR Lyrae (see text for a discussion), on an arbitrary vertical scale. The green region at $\phi < 0.15$ is the empirically determined region where abundance ratios appear to be poorly determined in some cases (see Section 4.5).

3.1 Use of static model atmospheres

The anomalous features of hydrogen absorption lines (emission, line doubling) in the spectra of RRab variables have been known for a long time (Struve 1947; Sanford 1949), and were attributed to the existence of shock waves at certain phases during the pulsation cycle, while there is no evidence to date of shock waves in the atmosphere of RRc stars. Studying this phenomenon requires spectroscopic observations with both high spectral and time resolution as well as high S/N, and until quite recently it could only be done on a small number of the nearest RRab variables with photographic spectra (Preston 1964; Preston & Paczynski 1964; Preston et al. 1965; Oke 1966), and later with electronic light detectors (Gillet & Crowe 1988; Gillet et al. 1989). The most accurate and detailed studies, however, were obviously done during the last decade thanks to the use of more advanced observation technology (Chadid et al. 2008; Kolenberg et al. 2010; For et al. 2011; Preston 2011).

Hydrodynamic model atmospheres (Hill 1972; Fokin 1992; Fokin et al. 1999) identify two pulsation phases where shocks occur: (i) the main shock corresponding to the so-called ‘hump’ at phase ~ 0.9 , when the infalling photosphere halts and its outward acceleration rapidly increases; and (ii) the early shock corresponding to the so-called ‘bump’ at phase ~ 0.7 , likely produced by colliding layers of material as the star approaches minimum radius (Gillet & Crowe 1988). Fig. 2 shows two spectra of our sample star VX Her, one taken in a shocked phase, the other in a quiescent phase. Although the shocks may fully develop in the higher atmospheric layers and hence mostly affect hydrogen lines (see e.g. Oke et al. 1992), they are also detectable at the photosphere, as shown by the broadening of photospheric FeI lines firstly observed by Lebre (1993, see also Clementini et al. 1994, and the quite long discussion on shocks presented in that paper). Both shocks are associated with the emission of ultraviolet excess energy, which is stronger at the 0.9 phase and weaker at the 0.7 phase, the origin of which has been attributed to various physical causes (see Smith 1995, for details).

Because static model atmospheres are more accurate and reliable than the available hydrodynamic ones, the general approach has been so far to restrict the analysis to the phase intervals in which the atmosphere is relatively stable. Traditionally, this has been chosen around phase $\phi \approx 0.75\text{--}0.80$ (see Figure 3), corresponding to the minimum of the typical light-curve of an ab-type RR Lyrae

⁵ <http://www.rotse.net/>

Table 3. 2MASS and extinction data used for determining the photometric temperatures listed in Table 5.

Star	2MASS designation	2MASS observation date (JD/BJD 2400000+)	$\phi_{2\text{MASS}}$ (mag)	$K_{2\text{MASS}}$ (mag)	A_V (mag)	A_K (mag)	$\langle K \rangle$ (mag)
DR And	J01051071+3413063	51105.8391/51105.84427	0.23	11.257	0.105	0.012	11.347
X Ari	J03083089+1026452	51519.7441/51519.74909	0.07	7.847	0.570	0.063	7.877
TW Boo	J14450595+4101442	50924.8937/50924.89713	0.79	10.378	0.041	0.004	10.248
TW Cap	J20142841-1350080	50968.9165/50968.92028	0.18	8.599	0.275	0.030	—
RX Cet	J00333827-1529147	51399.8505/51399.85440	0.63	10.338	0.078	0.009	10.298
U Com	J12400319+2729561	51525.0186/51525.01801	0.34	10.993	0.043	0.005	11.003
UZ CVn	J12302770+4030320	51647.8253/51647.82894	0.10	10.815	0.065	0.007	10.875
AE Dra	J18270674+5529327	51630.9614/51630.96115	0.81	11.308	0.104	0.011	11.138
BK Eri	J02495585-0125118	51116.6763/51116.68175	0.66	11.568	0.149	0.016	11.528
UY Eri	J03133913-1026323	51105.7000/51105.70486	0.10	9.893	0.184	0.020	—
SZ Gem	J07534345+1916240	50787.9584/50787.96258	0.93	10.845	0.121	0.013	10.745
VX Her	J16304079+1822005	51619.9286/51619.93043	0.22	9.508	0.133	0.015	9.588
DH Hya	J09001483-0946443	51197.6932/51197.69798	0.74	11.197	0.116	0.013	11.077
V Ind	J21112990-4504282	51403.7042/51403.70922	0.12	8.922	0.135	0.015	—
SS Leo	J11335449-0002000	51198.7677/51198.77106	0.44	9.880	0.056	0.006	9.935
V716 Oph	J16304946-0530195	51258.9032/51258.90542	0.55	9.862	1.202	0.132	—
VW Scl	J01181495-3912448	51118.5535/51118.55669	0.43	10.066	0.046	0.005	—
BK Tuc	J23293331-7232397	51528.5839/51528.58173	0.55	11.659	0.074	0.008	—
TU UMa	J11294849+3004025	50882.8692/50882.87440	0.76	8.857	0.064	0.007	8.747
RV UMa	J13331810+5359146	51566.9156/51566.91780	0.67	9.816	0.053	0.006	9.776
UV Vir	J12211673+0022029	51599.7621/51599.76715	0.58	10.946	0.073	0.008	10.946

Notes. 2MASS observation dates (JD) have been corrected to BJD using JSKyCalc (<http://www.dartmouth.edu/~physics/faculty/skycalc/flyer.html>). Extinction values (columns 6, 7) are from NED (<http://ned.ipac.caltech.edu/>) and are based on work by Schlafly & Finkbeiner (2011). $\langle K \rangle$ values have been calculated by us whenever possible from 2MASS data and K light curve templates for RR Lyrae by Jones et al. (1996).

star, although the region can only be defined with a certain level of approximation. More recently, Kolenberg et al. (2010) discussed the possibility that $\phi \approx 0.35$ also corresponds to a phase of quiescence, because RR Lyrae stars reach their minimum radius and for a short time we can safely use static model atmospheres (see Figure 3). Their statement is supported by the appearance of many iron lines with symmetric shapes in spectra of RR Lyrae observed in these phases, that can successfully be used for a chemical analysis (For et al. 2011).

From the empirical point of view, Clementini et al. (1995) performed abundance analysis of RR Lyrae spectra taken at or close to maximum light and For et al. (2011) and Wallerstein, Gomez, & Huang (2012) compared the abundance analysis of stars observed at different phases. Their conclusion is that reliable results can be obtained at almost all phases, provided that one avoids the narrow regions around shocks (see also Figure 3) and, of course, that exposure times are as short as possible to minimize the line shape deformations resulting from the overlap of different phases. In the sample presented here, a few stars have long exposure times (see Section 2.1) and a few exposures are into the dangerous zones presented in Figure 3. A discussion of these cases is postponed to Section 4.

As mentioned above, RRc variables do not show evidence of having shock phases, and the whole light curve is safe for abundance analysis (Govea et al. 2014). W Vir variables, instead, do have shocks. Maas et al. (2007) reject spectra which show line doubling, markedly asymmetric lines, or strong emission in the Balmer lines. According to those authors, spectra not showing these characteristics are likely to represent the atmosphere at a time when standard theoretical models may be applied. However, as stressed by Maas et al. (2007), this presumption should be tested by analysis of a series of spectra taken over the pulsation cycle: they ob-

tained consistent results from the analysis of a limited number of stars (three objects) with spectra taken at different phases. Among our programme stars, TW Cap is a W Vir star, while UY Eri and V716 Oph are BL Her variables. None of them exhibits strong profile alterations in their spectra, so we kept them in our sample.

3.2 Linelist and atomic data

To create a raw masterlist, we visually inspected the observed spectra, the solar spectrum by Moore et al. (1966), and a few synthetic spectra with temperatures ranging from 5000 to 7000 K, gravities ranging from 2.5 to 3.5 dex, and metallicities ranging from -2 dex to solar. The synthetic spectra were computed with Tsymbal's (Tsymbal 1996) LTE code. All visible lines that appeared not blended in at least one of the observed or theoretical spectra (considering also molecular lines in the theoretical spectra) where identified and included in the raw masterlist.

Atomic data for the selected lines were obtained from the VALD2⁶ and VALD3⁷ online databases (Kupka et al. 2000), including line broadening parameters, when available. The employed oscillator strengths ($\log gf$) and excitation potentials (χ_{ex}) are reported in Table 4, along with the measured EWs for each spectrum. More in detail, the major sources of $\log gf$ data for the selected lines are: for Fe the VALD2 critical compilation, based on 27 dif-

⁶ <http://vald.astro.univie.ac.at/~vald/php/vald.php>

⁷ <http://vald.astro.uu.se/>

Table 4. EWs and atomic data for individual program stars spectra.

Star	Spectrum	λ (Å)	Species	EW (mÅ)	δ EW (mÅ)	$\log gf$ (dex)	χ_{ex} (eV)
DR And	SARG1	4647.434	Fe I	58.20	7.11	-1.351	2.949
DR And	SARG1	4678.846	Fe I	43.30	8.60	-0.833	3.602
DR And	SARG1	4707.275	Fe I	40.70	5.00	-1.080	3.241
DR And	SARG1	4736.773	Fe I	40.50	4.42	-0.752	3.211
DR And	SARG1	4872.138	Fe I	89.20	4.96	-0.567	2.882
DR And	SARG1	4924.770	Fe I	41.30	6.30	-2.178	2.279

Note. Only a portion of this table is shown here for guidance regarding its form and content. A machine-readable version of the full table is available as supporting information with the online version of the paper.

ferent sources⁸; for Mg the Kurucz data (CD Rom 18)⁹; for Ca the Kurucz data (CD Rom 20-22); for Si the Kurucz data, from the 2007 set; for Ti I the Kurucz data (CD Rom 18); for Ti II Pickering, Thorne, & Perez (2001) and Wiese, Fedchak, & Lawler (2001); for Cr I and Cr II the Kurucz data (CD Rom 20-22); finally, for Ni both the Kurucz data (CD Rom 20-22) and the Fuhr, Martin, & Wiese (1988) data.

After the raw masterlist was assembled, an additional line selection was applied, based on empirical criteria. First, only lines that were actually measured in at least three different spectra (see next section) were retained and passed on through the abundance analysis. A further selection was performed iteratively after the abundance analysis rejection procedures (see Section 3.4), resulting in a final clean linelist of 352 lines of 9 species.

3.3 Equivalent widths

EW were then measured with the help of DAOSPEC (Stetson & Pancino 2008), run through the automated parameters optimizer DOOP (Cantat-Gaudin et al. 2014). In some cases the line profiles were deformed. For the long SARG exposure spectra, double peaks and asymmetric profiles were observed, owing to the integration along phases that in some cases were far from the equilibrium state. In all those cases, we forced DAOSPEC to adopt a radial velocity consistent with the deepest peaks, and the dominant line substructures. Clearly, the EW measurements by Gaussian fits were not optimal and this is reflected in the higher than usual (considering the S/N ratio) errors on the measurements, but also on the large uncertainties on the abundance results (see Section 3.4).

The way we used to measure EW has an impact on the resulting v_t of spectra with deformed line profiles: for those spectra where a “main” component could be identified, centered, and fit by the code, the FWHM would be relatively smaller, leading to a “normal” v_t , more similar to the field stars with unperturbed atmosphere. For those spectra with long exposure times, where the lines are also shallow and different atmospheric effects were included in the line profiles, a “global” Gaussian fit of all substructures would lead to a larger FWHM, and higher than usual resulting v_t . This is indeed the case, as discussed further in Section 4.3 and shown in Figure 5. However, the classical EW method implicitly tends to compensate for these effects, and as a result the iron abundances

are relatively stable and compare well with the literature (see also Sections 4.4 and 4.6).

The measured EW with their errors (as computed by DAOSPEC, see Stetson & Pancino 2008, for a detailed description) can be found in Table 4, where only lines surviving the described selection procedures are displayed.

3.4 Abundance computations

Abundance calculations were performed with GALA (Mucciarelli et al. 2013), which automatically finds the best atmospheric parameters and abundances, based on the Kurucz suite of abundance calculation programs (Kurucz 2005; Sbordone et al. 2004); we used the Atlas9 grid of atmospheric models computed by Castelli & Kurucz (2003)¹⁰. Briefly, GALA uses the classical method based on EW measurements, which refines an initial T_{eff} estimate by erasing any trend of iron abundance, $A(\text{Fe})$, with excitation potential; refines v_t by imposing that weak and strong lines give the same $A(\text{Fe})$; refines $\log g$ by minimizing the difference between $A(\text{FeI})$ and $A(\text{FeII})$; and finally, the method checks that there is no residual trend of $A(\text{Fe})$ with wavelength. Practically, as our spectral ranges included saturated telluric bands (after 6800 Å) that were difficult to remove, we ended up cutting the noisiest spectra after 5800 Å (in the worst cases) or 6500 Å (in the less bad cases).

GALA automatically selects lines based on three criteria: (i) their strength; (ii) their measurement error, provided by DAOSPEC in our case; and (iii) their discrepancy from the average $[\text{Fe}/\text{H}]$ of the other lines. In the last step of our raw master line list refinement, we rejected all those lines that survived GALA’s rejections in less than three spectra. After removing those lines from the master line list, we repeated both DAOSPEC (with its line selection) and GALA a few times, obtaining the final clean linelist described in Section 3.2 that was actually used for the final EW measurements and abundance analysis.

4 RESULTS

The results of our spectroscopic abundance analysis are reported in Tables 6 and 7 and discussed in the following sections, starting from the astrophysical parameter determination and following with the elements abundance ratios.

4.1 Effective temperature

To check that our spectroscopically derived effective temperatures are reasonable, we compared with two different estimates of the expected temperature at each phase, both based on photometry (see Figure 4).

The first method required an estimate of the infrared K magnitude at the phase of each spectroscopic observation. We used the Two Micron All Sky Survey (2MASS; Skrutskie et al. 2006) data and K light-curve templates from Jones et al. (1996) to obtain the K magnitudes of our programme stars at the phases of the spectroscopic observations, ϕ_{obs} . We adopted the V amplitudes listed in Table 1. We then derived the intrinsic $V - K$ color corresponding to our ϕ_{obs} , by adopting extinction values from Schlafly & Finkbeiner (2011) and ROTSE light curves. A few stars with no ROTSE light

⁸ See <http://vald.astro.univie.ac.at/~vald/php/vald.php?docpage=datasets.txt> for more information.

⁹ See <http://kurucz.harvard.edu/atoms/> for the complete collection of Kurucz atomic data.

¹⁰ <http://www.user.oat.ts.astro.it/castelli/>

Table 5. Photometric T_{eff} estimates from infrared 2MASS photometry (see Table 3) for a subset of programme stars.

Star	Spectrum	ϕ_{obs}	K_{obs}	V_{obs}	T_{eff}
DR And	SARG 1	0.63	11.380	12.795	6058
	SARG 2	0.69	11.405	12.813	6070
	SARG 3	0.31	11.264	12.543	6294
X Ari	APO 1	0.19	7.818	9.381	6607
TW Boo	SARG 1	0.61	10.254	11.575	6129
	SARG 2	0.65	10.275	11.575	6166
	SARG 3	0.69	10.300	11.590	6183
RX Cet	SARG 1	0.51	10.281	11.586	6186
U Com	SARG 1	0.87	11.013	11.323	8460
	SARG 2	0.95	10.843	11.269	8106
	SARG 3	0.02	10.843	11.269	8106
UZ CVn	SARG 1	0.04	10.825	11.778	6955
	SARG 2	0.08	10.817	11.852	6775
	SARG 3	0.13	10.808	11.921	6611
AE Dra	SARG 1	0.05	11.088	12.087	6899
	SARG 2	0.10	11.071	12.218	6588
BK Eri	UVES 1	0.04	11.495	12.320	7361
	UVES 2	0.20	11.445	12.599	6628
	UVES 3	0.14	11.461	12.524	6816
	UVES 4	0.51	11.511	12.919	6152
SZ Gem	SARG 1	0.50	10.712	12.079	6183
VX Her	SARG 1	0.86	9.796	11.127	6245
	SARG 2	0.05	9.541	10.213	7673
DH Hya	UVES 1	0.79	11.219	12.627	6107
	SARG 1	0.71	11.152	12.537	6147
SS Leo	SARG 2	0.79	11.219	12.627	6107
	UVES 1	0.06	9.880	10.714	7163
TU UMa	UVES 2	0.07	9.887	10.732	7138
	SARG 1	0.45	8.705	9.954	6302
RV UMa	SARG 1	0.62	9.801	11.168	6050
	SARG 2	0.66	9.818	11.174	6068
	SARG 3	0.71	9.851	11.198	6083
UV Vir	UVES 1	0.87	11.146	12.218	6666

curves and Population II Cepheids were excluded at this stage. Lastly, we used the empirical calibration of T_{eff} versus colour by Alonso et al. (1999, their equation 8)¹¹ to derive the T_{eff} values.

The T_{eff} values for the subset of our programme stars for which it was possible to apply the method outlined above, are listed in Table 5. An estimate of the typical uncertainty on the 2MASS photometric T_{eff} was obtained by propagating the reference magnitudes uncertainties, and resulted of ≈ 220 K. The average difference between these T_{eff} values and the corresponding ones derived from spectroscopy is $\langle \Delta T_{\text{eff}} \rangle = 71 \pm 382$ K.

For a second comparison, we used the temperatures of the eight stars used by For et al. (2011) for creating their T_{eff} -phase relations. Their photometric temperatures (derived from B-V, V-R_c, and V-I_c colors) are used to derive a region of confidence, shown in Figure 4 as a blue shaded area. We also used the final T_{eff} derived by For et al. (2011) for their programme stars (including uncertainties), to derive an additional region of confidence (red shaded area in Figure 4). The two regions together cover a similar parameter space as that covered by our targets, both in metallicity and in pe-

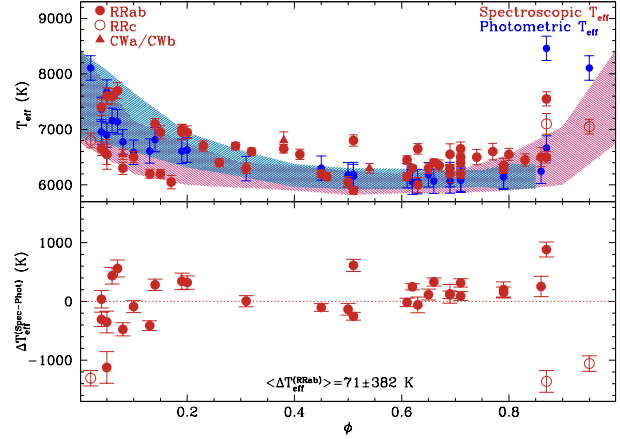


Figure 4. *Top panel:* comparison of our spectroscopic T_{eff} (red symbols, where filled circles represent RRab, empty circles RRC, and filled triangles Population II Cepheids) with photometric ones. The blue circles are derived from 2MASS colors (see text and Table 5) while the shaded areas represent different estimates from For et al. (2011): the blue shaded region roughly covers the T_{eff} values of their eight comparison stars, while the red shaded region roughly covers the T_{eff} values of their programme stars (including uncertainties). *Bottom panel:* difference (red symbols) between the spectroscopic and the 2MASS photometric T_{eff} estimates.

riod. Our spectroscopically derived T_{eff} values mostly fall inside or near the borders of the shaded areas.

We note that the spectrum of UV Vir, taken dangerously close to the main shock zone, needed a higher than expected T_{eff} to converge, but gravity and microturbulence still appear reasonable. A special discussion deserves the case of U Com, the only type RRc variable, which displays a much lower spectroscopic temperature (by more than 1000 K) than the photometric estimates, being more in line with the temperatures expected for other RRab variables in the sample. The only other high-resolution studies of RRc variables, to our knowledge, are: Lambert et al. (1996, containing DH Peg and T Sex) and Govea et al. (2014, who specifically targeted eight RRc stars). Neither of these studies, covering altogether a larger metallicity range than ours, report $T_{\text{eff}} > 7600$ K; in particular, Figure 11 by Govea et al. (2014) illustrates the variation of their spectroscopic T_{eff} as a function of phase: for the phases of our three spectra of U Com, we should expect $7000 < T_{\text{eff}} < 7500$ K, roughly. We are thus confident that our T_{eff} for this star are roughly correct. As supporting evidence, we note that the resulting [Fe/H] for U Com is only 0.2 dex lower than the Beers et al. (2000) estimate.

In conclusion, our spectroscopically derived T_{eff} values agree with the values that are, roughly speaking, expected judging from optical (For et al. 2011) and infrared (2MASS) photometry, except for a marginal discrepancy for some stars around $0.3 < \phi < 0.4$ and $0.6 < \phi < 0.8$. The T_{eff} obtained for each spectrum, along with the error estimated by GALA (see Mucciarelli et al. 2013, for more details) from the slope of [Fe/H] versus excitation potential, are listed in Table 6.

4.2 Surface gravity

The acceleration term that is needed to account for the dynamic atmosphere of RR Lyrae (Clementini et al. 2005) can be determined by differentiating the radial velocity curve, which is a basic ingre-

¹¹ Two stars have some spectra just outside the limits of applicability of this calibration, having $(V-K) < 0.1$ mag: AE Dra (at $\phi=0.05$) and BK Eri (at $\phi=0.04$ and 0.14). However, given the large uncertainties involved in the procedure and our use of photometric temperatures just as a reference value, we chose to use formula 8 by Alonso et al. (1999) in any case.

Table 6. Adopted atmospheric parameters and resulting iron abundances.

Star	Spectrum	T_{eff} (K)	δT_{eff} (K)	$\log g$ (dex)	$\delta \log g$ (dex)	v_t (km/s)	δv_t (km/s)	[FeI/H] (dex)	σ [FeI/H] (dex)	∂ [FeI/H] (dex)	[FeII/H] (dex)	σ [FeII/H] (dex)	∂ [FeII/H] (dex)
DR And	SARG 1	6000	134	1.60	0.10	2.7	0.2	-1.40	0.19	0.07	-1.45	0.03	0.03
	SARG 2	6200	160	2.30	0.17	2.9	0.4	-1.53	0.17	0.07	-1.61	0.07	0.03
	SARG 3	6300	95	2.10	0.14	2.4	0.2	-1.29	0.12	0.07	-1.33	0.13	0.03
X Ari	APO 2	6950	141	3.10	0.38	2.2	0.5	-2.19	0.17	0.17	-2.10	0.23	0.13
TW Boo	SARG 1	6150	71	2.00	0.09	2.1	0.2	-1.49	0.12	0.07	-1.45	0.11	0.04
	SARG 2	6300	93	2.30	0.06	2.2	0.2	-1.39	0.14	0.07	-1.37	0.03	0.04
	SARG 3	6300	64	2.10	0.07	2.6	0.3	-1.49	0.11	0.07	-1.49	0.33	0.03
TW Cap	UVES 1	6300	86	1.10	0.08	1.9	0.2	-1.63	0.10	0.07	-1.68	0.07	0.04
RX Cet	SARG 1	6800	103	2.00	0.12	1.7	0.2	-1.38	0.13	0.07	-1.39	0.09	0.04
U Com	SARG 1	7100	186	2.30	0.18	1.5	0.2	-1.44	0.14	0.07	-1.43	0.16	0.05
	SARG 2	7050	133	2.30	0.15	1.6	0.2	-1.38	0.16	0.07	-1.41	0.10	0.05
	SARG 3	6800	132	2.20	0.20	1.5	0.2	-1.42	0.15	0.06	-1.41	0.17	0.05
UZ CVn	SARG 1	6650	122	2.40	0.08	1.3	0.3	-2.05	0.22	0.07	-2.11	0.04	0.04
	SARG 2	6300	112	2.30	0.08	1.5	0.3	-2.22	0.12	0.07	-2.19	0.04	0.03
	SARG 3	6200	82	2.30	0.14	1.3	0.3	-2.30	0.15	0.07	-2.27	0.11	0.03
AE Dra	SARG 1	6550	184	1.90	0.11	1.6	0.2	-1.51	0.18	0.07	-1.45	0.10	0.04
	SARG 2	6500	102	1.80	0.19	1.6	0.2	-1.44	0.15	0.07	-1.42	0.12	0.04
BK Eri	UVES 1	7400	150	2.20	0.20	1.7	0.2	-1.87	0.21	0.07	-1.89	0.19	0.04
	UVES 2	6950	114	2.30	0.07	2.2	0.3	-1.54	0.12	0.08	-1.52	0.07	0.04
	UVES 3	7100	98	1.90	0.24	1.2	0.3	-1.51	0.15	0.07	-1.57	0.15	0.04
	UVES 4	5900	67	1.60	0.06	1.6	0.1	-1.85	0.11	0.08	-1.84	0.07	0.03
UY Eri	SARG 1	6800	157	1.80	0.08	1.6	0.4	-1.43	0.19	0.07	-1.48	0.07	0.04
SZ Gem	SARG 1	6050	101	1.90	0.10	1.5	0.1	-1.65	0.13	0.07	-1.59	0.10	0.04
VX Her	SARG 1	6500	172	1.90	0.09	2.3	0.2	-1.49	0.10	0.07	-1.51	0.05	0.04
	SARG 2	6550	268	2.20	0.11	2.3	1.1	-1.73	0.19	0.06	-1.76	0.03	0.04
DH Hya	UVES 1	6300	93	2.10	0.13	1.9	0.2	-1.52	0.12	0.07	-1.52	0.15	0.04
	SARG 2	6200	76	2.10	0.17	1.6	0.2	-1.55	0.16	0.07	-1.54	0.14	0.04
	SARG 3	6350	129	1.80	0.35	2.1	0.2	-1.48	0.20	0.07	-1.55	0.26	0.05
V Ind	UVES 1	7000	86	2.30	0.11	1.6	0.1	-1.33	0.08	0.07	-1.31	0.12	0.03
	UVES 2	6700	67	2.20	0.08	1.9	0.1	-1.43	0.07	0.07	-1.41	0.07	0.03
	FEROS 1	6150	72	1.70	0.05	1.8	0.1	-1.56	0.09	0.07	-1.59	0.05	0.04
	FEROS 2	6450	74	2.40	0.08	1.9	0.1	-1.30	0.12	0.07	-1.33	0.11	0.03
	FEROS 3	6650	95	2.60	0.10	1.9	0.2	-1.20	0.23	0.06	-1.19	0.04	0.04
	HARPS 1	6350	100	1.50	0.61	1.5	0.2	-1.28	0.16	0.07	-1.30	0.21	0.04
	HARPS 2	6550	206	2.30	0.93	2.8	0.3	-1.17	0.10	0.06	-1.18	0.30	0.04
	HARPS 3	6650	122	2.50	0.13	2.0	0.2	-1.10	0.20	0.06	-1.18	0.19	0.03
	HARPS 4	6650	75	2.50	0.08	1.4	0.1	-1.25	0.09	0.06	-1.24	0.13	0.03
	HARPS 5	6550	92	2.50	0.09	1.8	0.1	-1.18	0.09	0.06	-1.21	0.11	0.04
	HARPS 6	6500	135	2.50	0.17	2.8	0.3	-1.30	0.27	0.07	-1.37	0.04	0.04
	HARPS 7	6600	149	2.30	0.22	2.7	0.2	-1.16	0.23	0.06	-1.14	0.18	0.04
	HARPS 8	6550	108	2.60	0.18	2.7	0.3	-1.23	0.25	0.06	-1.25	0.14	0.04
	HARPS 9	6450	112	2.10	0.20	2.8	0.2	-1.34	0.19	0.07	-1.39	0.17	0.04
	HARPS 10	6500	103	2.30	0.26	2.3	0.2	-1.43	0.17	0.07	-1.55	0.15	0.04
SS Leo	UVES 1	7600	140	2.50	0.07	1.1	1.1	-1.49	0.08	0.18	-1.47	0.05	0.13
	UVES 2	7700	145	2.50	0.07	1.6	1.0	-1.46	0.07	0.19	-1.46	0.06	0.16
V716 Oph	UVES 1	6550	91	2.50	0.09	1.6	0.1	-1.87	0.08	0.07	-1.87	0.07	0.03
VW Scl	UVES 1	6400	76	2.50	0.09	2.4	0.2	-1.18	0.11	0.07	-1.26	0.11	0.03
	UVES 2	6700	94	2.10	0.08	1.9	0.1	-1.32	0.08	0.07	-1.31	0.06	0.04
	UVES 3	6600	64	2.30	0.11	1.7	0.1	-1.16	0.10	0.06	-1.23	0.12	0.04
	UVES 4	6950	118	2.30	0.17	1.7	0.2	-1.30	0.10	0.07	-1.30	0.11	0.04
	UVES 5	7600	150	2.30	0.20	1.6	0.2	-1.46	0.15	0.09	-1.43	0.10	0.04
BK Tuc	UVES 1	6050	120	1.90	0.11	2.4	0.1	-1.80	0.10	0.08	-1.76	0.06	0.04
	UVES 2	6400	68	2.30	0.10	2.3	0.4	-1.60	0.11	0.07	-1.63	0.08	0.05
	UVES 3	6200	79	2.00	0.08	2.1	0.1	-1.62	0.12	0.07	-1.65	0.08	0.04
TU UMa	SARG 1	6200	65	2.10	0.15	1.8	0.2	-1.31	0.14	0.07	-1.32	0.15	0.02
RV UMa	SARG 1	6300	53	2.20	0.10	1.6	0.1	-1.27	0.12	0.06	-1.23	0.13	0.04
	SARG 2	6400	69	2.30	0.12	1.8	0.1	-1.16	0.10	0.07	-1.16	0.14	0.05
	SARG 3	6400	71	2.30	0.12	1.9	0.1	-1.13	0.13	0.06	-1.20	0.12	0.03
UV Vir	UVES 1	7550	128	2.10	0.16	1.3	0.3	-1.10	0.10	0.09	-1.23	0.25	0.04

Notes. For each star and each spectrum, the columns report T_{eff} , $\log g$, and v_t obtained with GALA with their formal errors, followed by the average [FeI/H] and [FeII/H] obtained from all Fe I and Fe II surviving lines, their spreads σ [FeI/H] and σ [FeII/H], and their sensitivity ∂ [FeI/H] and ∂ [FeII/H] to variations of the atmospheric parameters (see text for more details).

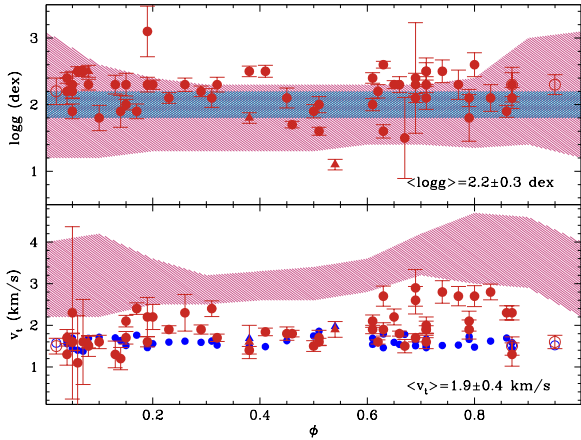


Figure 5. Comparison of our spectroscopic $\log g$ (red symbols, upper panel) and v_t (red symbols, bottom panel) with different literature reference values. The red shaded regions represent roughly the final values obtained by For et al. (2011), including their uncertainties. The blue shaded strip in the upper panel shows the theoretical (fixed) $\log g$ adopted by For et al. (2011) to build their synthetic spectra. The blue filled circles in the lower panel show v_t values obtained for our programme stars using the GES (Gaia-ESO Survey) relation (see text) for non-variable stars.

dient in the Baade-Wesselink method¹². The effect of the early and main shocks can be computed (see for example the computations for S Arae by Chadid et al. 2008, their Figure 3). In general, the acceleration associated with the main shock should produce a significant increase of the effective gravity with respect to the static value, $\Delta \log g \approx 0.6\text{--}0.8$ dex, whereas the acceleration associated with the early shock should affect the gravity only marginally, by ≤ 0.1 dex. Apart from the absolute values of the gravity, which depend on the assumed stellar mass and radius, the effective gravity/acceleration curves show that the only part of the pulsation cycle where gravity can be significantly different from the static value is around the maximum light (approximately minimum radius) phase. Recent model computations by Kolenberg et al. (2010) and observed spectra analysis by For et al. (2011) show that assuming a constant gravity throughout the pulsation cycle is appropriate (within 0.1 dex).

We used the spectroscopic method to balance Fe I and Fe II and our derived gravities distribute flatly around $\langle \log g \rangle = 2.2 \pm 0.3$ dex (see Table 6 and Figure 5) and show no significant trend with phase. In particular, we note that four of our spectra are taken in the shocked zone with $0.85 < \phi < 1.0$ ¹³, but none displays largely deviant gravities. A large scatter is anyway present, undoubtedly caused by the paucity of very reliable Fe II lines away from the optimal phases: X Ari displays a very high $\log g = 3.1 \pm 0.38$ dex, for that reason.

Our $\log g$ values are broadly compatible with the ones found by For et al. (2011), and are substantially lower than those obtained in past high-resolution studies (Butler et al. 1979; Clementini et al. 1995; Lambert et al. 1996), which were closer to 3 dex and in general to the B-W determinations of gravity. Explanations for this

difference were searched by For et al. (2011), who invoked uncertainties on the NLTE corrections (see also Clementini et al. 1995; Lambert et al. 1996): NLTE effects should in principle produce lower gravities when one obtains gravity by forcing Fe I and Fe II to be as close as possible¹⁴. While further investigation of NLTE effects in the atmospheres of RR Lyrae stars would be highly desirable, past studies (see for example Lambert et al. 1996) do support the idea that a 0.5–1.0 dex difference in $\log g$ could be induced by NLTE effects. Because the LTE spectroscopic $\log g$ values could be in principle indicative of NLTE effects, the fact that we do not observe significant $\log g$ changes with phase (nor with $[\text{Fe}/\text{H}]$), is suggestive of a relatively small NLTE effect, contained within roughly 0.2 dex in terms of Fe I, unless other effects occurring in the complex atmospheres of these stars act to mask NLTE effects: for example, the large discrepancy in the behaviour of $\log g$ along the pulsation cycle found with the B-W method (see above) and with high-resolution spectroscopic analysis, is clearly not understood yet.

We also studied the impact of adopting different Fe II $\log gf$ (Fe I atomic data are overall more reliable), that are a well known source of uncertainty in this type of analysis (Meléndez & Barbuy 2009). We measured an average difference between the present study and the one by Clementini et al. (1995) — as an example — of $\langle \log gf \rangle = +0.06 \pm 0.18$ dex¹⁵. We thus tried changing our $\log gf$ on our highest S/N spectrum (TW Cap) by that amount and allowed for GALA to re-converge with the new Fe II $\log gf$ values and the same EWs. As a result, $\log g$ was raised by only 0.2 dex, with T_{eff} untouched and v_t raised by 0.2 km/s. While these changes go in the right direction to reconcile the mentioned studies, they are largely insufficient to explain the said differences.

To preserve the internal consistency of our analysis, and supported by the findings by For et al. (2011), we used the $\log g$ spectroscopic values obtained by enforcing Fe ionization equilibrium, which are listed in Table 6, along with the error estimated by GALA (see Mucciarelli et al. 2013, for more details) from the difference between $[\text{Fe}/\text{H}]$ and $[\text{FeII}/\text{H}]$.

4.3 Microturbulent velocity

As discussed in Section 3.3, the method we use for measuring EWs has an impact on our resulting v_t values obtained by balancing $[\text{Fe}/\text{H}]$ with EW. There are three cases: (i) the line profiles are not distorted and the Gaussian fit is a good approximation; (ii) the line profiles are mildly asymmetric when the atmosphere is not static, thus DAOSPEC could still fit Gaussians with a slightly higher FWHM to include the whole line structure, obtaining a reasonably reliable EW; (iii) the line profiles are heavily distorted, for example because of a long exposure time, including different phases where the line structures change rapidly, and DAOSPEC was forced to fit the “main” component of the line with a Gaussian, neglecting or leaving out secondary components or asymmetric wings: the adopted FWHM is not much higher than what expected for a non-variable star with similar characteristics¹⁶. It is important to recall at this point that the method employed by For et al. (2011) was to

¹² We found that a few of our programme stars were previously analysed with the Baade-Wesselink method, based on very accurate visual and infrared light curves; these are X Ari (Fernley et al. 1989), V Ind (Clementini, Cacciari, & Lindgren 1990) and TU UMa (Liu & Janes 1990).

¹³ They are: the second and third SARG spectra of U Com, the second SARG spectrum of VX Her, and the first UVES spectrum of V Ind.

¹⁴ This is because LTE abundances of Fe I should be lower than those of Fe II, and to compensate that, a lower gravity would be needed in an LTE analysis (see also Allende Prieto et al. 1999).

¹⁵ Our $\log gf$ scale for Fe II is 0.05 ± 0.08 dex lower, on average, than that of Meléndez & Barbuy (2009).

¹⁶ It is interesting to note here that the expected axis rotation of RRab stars does not generally exceed $v_{\text{rot}} \sin i = 6$ km/s (see Preston & Chadid 2013, and references therein), thus it is not surprising that isolating the “main” Gaus-

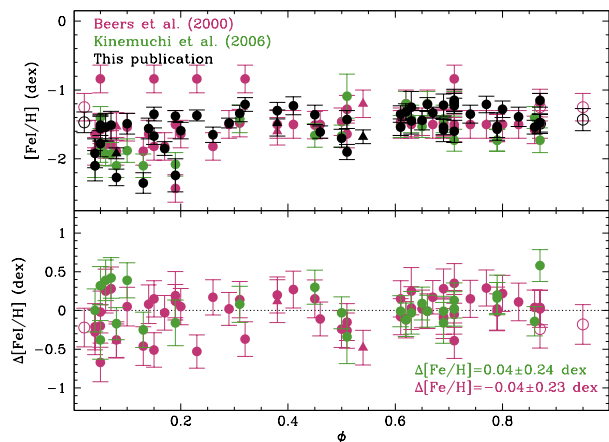


Figure 6. Comparison of our spectroscopic $[\text{Fe}/\text{H}]$, plotted in black, with Beers et al. (2000), plotted in magenta, and Kinemuchi et al. (2006), plotted in green. The symbols are the same as in Figs 4 and 5. The top panel shows the absolute values and the bottom panel the differences, in the sense of our measurements minus the literature ones, as a function of phase.

integrate the heavily distorted lines instead of fitting them with a Gaussian: this explains their v_t values, higher than those of non-variable field stars with similar characteristics.

As can be seen in Figure 5, our resulting v_t values are mostly similar to the ones expected for non-pulsating field stars, on the basis of the Gaia-ESO survey v_t relation (Bergemann et al, in preparation), and sometimes higher, almost as high as those by For et al. (2011). The low values correspond to cases (i) and (iii) listed above, while the intermediate or high values correspond to case (ii) above. We rarely reach as high values as For et al. (2011) or predicted by Fokin et al. (1999), because we rarely use the whole line profile for our abundance analysis. It is important to note, however, that both methods for measuring EW produce reliable iron abundances, because with both the adopted abundance analysis method ensures self-consistency (though parameters inter-dependence) in this respect. The large scatter of parameters in our case does, however, imply a larger uncertainty for these variable stars compared with non-variable stars observed with similar spectral quality (see below).

The v_t obtained for each spectrum, along with the error estimated by GALA (see Mucciarelli et al. 2013, for more details) from the slope of the relation between $[\text{Fe}/\text{H}]$ and EW, are listed in Table 6.

4.4 Iron abundance

We derived our Fe I and Fe II abundances as the median of all the available iron lines, generally of the order of ≈ 70 –90 Fe I and ≈ 10 Fe II surviving lines. As we generally achieved a good ionization balance between Fe I and Fe II ($\Delta[\text{Fe}/\text{H}]$ was typically 0.01 ± 0.04 dex, ranging from -0.09 to $+0.13$ dex), we used Fe I to define $[\text{Fe}/\text{H}]$. We do not detect very large non-LTE effects, that with our method would appear as very low gravities, but according to Lambert et al. (1996) and Clementini et al. (1995) these should be either of the order of 0.2 dex or negligible, respectively, and

sian component of a multiple or asymmetric line profile produces FWHM values not much higher than the ones expected from the spectral resolution.

thus could imply some ≈ 0.5 –1.0 dex underestimate of the surface gravities (see also the discussion in Section 4.2).

We compared our results with the two studies by Kinemuchi et al. (2006) and Beers et al. (2000). The former study used both the Jurcsik & Kovacs (1996) and the Sandage (2004) calibrations of RR Lyrae metallicities as a function of the period and the Fourier ϕ_{31} parameter. The latter study was instead based on the Beers et al. (1999) recalibration of their prism survey to search for metal-poor stars using the calcium K line. Both literature calibrations are thus based on solar abundance values around $A(\text{Fe})_\odot = 7.55$ –7.50 and thus should agree well with our adopted solar composition (Grevesse & Sauval 1998). For a more detailed comparison with high-resolution spectroscopic studies, see Section 4.6.

As shown in Figure 6, this is indeed the case: our values show no significant offset with the two cited studies, and no significant trends with phase are observed¹⁷. The difference with Beers et al. (2000) is $\langle \Delta[\text{Fe}/\text{H}] \rangle = -0.04 \pm 0.23$ dex, in the sense that our $[\text{Fe}/\text{H}]$ values are slightly lower than theirs; the difference with Kinemuchi et al. (2006) is $\langle \Delta[\text{Fe}/\text{H}] \rangle = +0.04 \pm 0.24$ dex. Beers et al. (2000) report an error on their estimates of 0.1–0.2 dex, while Kinemuchi et al. (2006) reported a scatter of the order of 0.3 dex. The comparison shows that our global errors on $[\text{Fe}/\text{H}]$ of each single spectrum should be — roughly speaking — 0.10–0.15 dex at most. Given the variety of $[\text{Fe}/\text{H}]$ calibrations for RR Lyrae in the literature, all having reported uncertainties roughly around 0.2–0.3 dex (for example Catelan 1992; Sandage 1993; Jurcsik & Kovacs 1996; Alcock et al. 2000; Sandage 2004; Bono, Caputo, & Di Criscienzo 2007, to name a few) we can conclude that the agreement found in the metallicity range covered in this paper is more than satisfactory. Also, being the present work one of the few based on high resolution spectroscopy ($R \geq 30\,000$, see also references in Section 4.6), this lends independent support to those calibrations, at least in the explored metallicity range.

The average Fe I and Fe II abundances of the surviving lines in each spectrum can be found in Table 6, together with their spreads ($\sigma[\text{FeI}/\text{H}]$ and $\sigma[\text{FeII}/\text{H}]$) and their sensitivity to a variation of ± 100 K in T_{eff} , ± 0.1 dex in $\log g$, and ± 0.1 km/s in v_t ($\partial[\text{FeI}/\text{H}]$ and $\partial[\text{FeII}/\text{H}]$, computed by summing in quadrature the abundance variations obtained by varying each parameter separately). As can be seen, Fe I is generally twice as sensitive to parameters variations than Fe II.

The final Fe abundance for each star was computed as the weighted average of the Fe I measurements for each epoch, using as weights $w = 1/\delta[\text{FeI}/\text{H}]^2$, where $\delta[\text{FeI}/\text{H}]$ was computed by summing in quadrature the random error $\sigma[\text{FeI}/\text{H}]/\sqrt{n}$ ¹⁸ and the variations of $[\text{FeI}/\text{H}]$ obtained by altering the atmospheric parameters by their errors, as listed in Table 6. The result is shown in Table 7.

4.5 Abundance ratios

Abundance ratios for a few elements other than iron were computed for each spectrum, providing uncertainties and final star weighted averages in the same way used for iron (see Table 7). The behaviour

¹⁷ A small oscillation can be picked up by the eye, with an amplitude of $\lesssim 0.1$ dex, almost hidden within the scatter. While the oscillation is not statistically significant with the data in hand, it still suggests that the use of spectra at different phases is risky when an error below 0.1 dex is needed.

¹⁸ n is the number of surviving Fe I lines in each spectrum.

Table 7. Abundance ratios.

Star	[Fe/H] (dex)	[Mg/Fe] (dex)	[Ca/Fe] (dex)	[Si/Fe] (dex)	[Ti/Fe] (dex)	[Cr/Fe] (dex)	[Ni/Fe] (dex)
DR And	-1.37 ± 0.12	0.39 ± 0.41	0.24 ± 0.19	0.67 ± 0.21	0.20 ± 0.14	-0.11 ± 0.26	0.09 ± 0.20
X Ari	-2.19 ± 0.17	0.50 ± 0.08	0.27 ± 0.11	...	0.73 ± 0.62	-0.10 ± 0.40	0.30 ± 0.10
TW Boo	-1.47 ± 0.05	0.24 ± 0.10	0.24 ± 0.07	0.69 ± 0.02	0.20 ± 0.13	0.03 ± 0.17	0.07 ± 0.04
TW Cap	-1.63 ± 0.06	0.75 ± 0.07	0.28 ± 0.06	0.82 ± 0.19	0.20 ± 0.07	-0.02 ± 0.13	-0.04 ± 0.06
RX Cet	-1.38 ± 0.07	0.60 ± 0.12	0.18 ± 0.07	0.80 ± 0.18	0.11 ± 0.23	-0.02 ± 0.08	-0.04 ± 0.07
U Com	-1.41 ± 0.03	0.33 ± 0.19	0.23 ± 0.05	0.89 ± 0.35	0.18 ± 0.11	0.01 ± 0.09	0.05 ± 0.04
UZ CVn	-2.21 ± 0.13	0.48 ± 0.08	0.50 ± 0.24	1.43 ± 0.12	0.38 ± 0.18	0.09 ± 0.34	0.36 ± 0.52
AE Dra	-1.46 ± 0.05	0.46 ± 0.05	0.19 ± 0.04	1.08 ± 0.01	0.19 ± 0.19	0.28 ± 0.22	0.18 ± 0.16
BK Eri	-1.72 ± 0.21	0.46 ± 0.14	0.23 ± 0.15	0.52 ± 0.20	0.12 ± 0.27	-0.04 ± 0.19	-0.05 ± 0.34
UY Eri	-1.43 ± 0.11	0.41 ± 0.08	0.20 ± 0.11	0.42 ± 0.24	0.17 ± 0.27	-0.01 ± 0.11	0.05 ± 0.13
SZ Gem	-1.65 ± 0.07	0.51 ± 0.08	0.34 ± 0.07	0.61 ± 0.10	0.12 ± 0.25	-0.02 ± 0.29	-0.11 ± 0.10
VX Her	-1.56 ± 0.17	0.17 ± 0.22	0.18 ± 0.25	1.17 ± 0.45	0.01 ± 0.22	0.08 ± 0.28	0.15 ± 0.05
DH Hya	-1.53 ± 0.01	0.38 ± 0.10	0.31 ± 0.04	0.63 ± 0.31	0.13 ± 0.20	0.03 ± 0.17	0.16 ± 0.05
V Ind	-1.30 ± 0.14	0.41 ± 0.12	0.23 ± 0.11	0.46 ± 0.29	0.15 ± 0.19	-0.06 ± 0.14	-0.10 ± 0.15
SS Leo	-1.48 ± 0.07	0.41 ± 0.13	0.35 ± 0.10	...	0.20 ± 0.06	-0.05 ± 0.05	0.87 ± 0.21
V716 Oph	-1.87 ± 0.06	0.51 ± 0.04	0.34 ± 0.05	0.59 ± 0.05	0.35 ± 0.13	0.01 ± 0.04	0.06 ± 0.10
VW Scl	-1.22 ± 0.10	0.38 ± 0.10	0.22 ± 0.12	0.47 ± 0.06	0.23 ± 0.30	-0.08 ± 0.12	-0.10 ± 0.07
BK Tuc	-1.65 ± 0.09	0.57 ± 0.11	0.32 ± 0.09	0.38 ± 0.06	0.13 ± 0.12	-0.11 ± 0.09	0.01 ± 0.08
TU UMa	-1.31 ± 0.05	0.29 ± 0.03	0.25 ± 0.04	0.28 ± 0.05	0.18 ± 0.08	-0.13 ± 0.06	-0.23 ± 0.05
RV UMa	-1.20 ± 0.08	0.31 ± 0.07	0.25 ± 0.08	0.46 ± 0.11	0.22 ± 0.11	-0.12 ± 0.11	-0.20 ± 0.08
UV Vir	-1.10 ± 0.12	0.69 ± 0.10	0.41 ± 0.13	...	0.10 ± 0.04	-0.10 ± 0.08	0.04 ± 0.13

of abundance ratios with phase is illustrated in Figure 7. The resulting abundance ratios are also plotted in Figure 8 versus [Fe/H].

In summary, in spite of the obvious difficulties of obtaining parameters and abundance ratios on variable stars spectra, especially when one observes with long exposure times or outside the optimal phases, the results are stable and broadly comparable to those obtained for non-variable stars *even rather close to the shock phases*, if some extra effort is put into a careful selection of spectral lines (we used an outlier rejection) and if one accepts the inevitably higher errors and scatter (of the order of 0.1–0.15 dex, roughly speaking) compared to non-variable stars. In other words, the classical EW method based on static atmosphere models still works over most of the pulsation cycle, including the early and main shock regions. However, immediately after the main shock phase, we note a dangerous zone lying roughly within $0 \lesssim \phi \lesssim 0.15$, depending on the species (see Figure 7), which appears indeed to be the region where the maximum disturbance on abundance determinations is reached. Our work fully supports the findings by Clementini et al. (1995), For et al. (2011) or Wallerstein, Gomez, & Huang (2012), and adds more insight into the main shock phase, where indeed some neutral lines start disappearing (Chadid et al. 2008), but other lines appear to remain reliable.

4.5.1 Iron-peak elements

The iron-peak elements abundances of chromium and nickel (Table 7), are based on approximately 5–15 well-behaved lines for each element (see also Table 4 for a list of surviving lines), depending on the spectrum. The scatter seems to increase for a few spectra immediately after the main shock phase, and there are a few outliers, but when all measurements for a star are combined through a weighted average, the resulting abundance ratios are rather compatible with solar values, within the highly varying uncertainties (Figure 8): the weighted averages are $\langle[\text{Ni}/\text{Fe}]\rangle = 0.08 \pm 0.18$ dex

and $\langle[\text{Cr}/\text{Fe}]\rangle = -0.01 \pm 0.11$ dex¹⁹. Unlike For et al. (2011), we do not find a large discrepancy between Cr I and Cr II: $\langle\Delta[\text{Cr}/\text{Fe}]\rangle = -0.11 \pm 0.11$ dex, but we observe that the difference increases after the main shock phase (Figure 7) and around and after the early shock phase, and that it goes in the same sense as theirs (see also Clementini et al. 1995; Sobeck, Lawler, & Sneden 2007). The two most metal-poor stars, X Ari and UZ CVn, display rather large errorbars — owing most certainly to the paucity of lines — but, for example, their enhanced nickel abundance is in line with what found by Gratton et al. (2003) for field stars.

4.5.2 α -elements

We also provide abundance ratios for Mg I, Ca I, Si I, Ti I, and Ti II (Table 7), based on approximately 3, 30, 10, 10, and 20 lines, respectively (see Table 4). Unlike the two iron-peak elements studied above, calcium and magnesium do not seem to display any increase in the scatter after the main shock, although there is a hint of a decrease in their abundance before the shock (see also Chadid et al. 2008).

Silicon, which was extensively discussed by For et al. (2011), appears indeed extremely sensitive to the phase, with a larger spread at all phases and very roughly following the T_{eff} trend. It was previously reported in the literature (Shi et al. 2009), that silicon lines have largely different NLTE effects and that bluer lines should have larger effects in general with respect to redder lines. Our selection of lines (reported in Table 4), is based on the EW measurement quality and on statistical rejections within the GALA routines, thus displaying a rough average effect, with a large spread.

Apart from a few outliers, titanium behaves similarly to magnesium and calcium; we can also observe a constant offset between Ti I and Ti II, of 0.18 ± 0.10 dex, with Ti I higher than Ti II. As discussed extensively by For & Sneden (2010) and For et al. (2011),

¹⁹ [Cr/Fe] was obtained as the weighted average of [Cr I/Fe] and [Cr II/Fe].

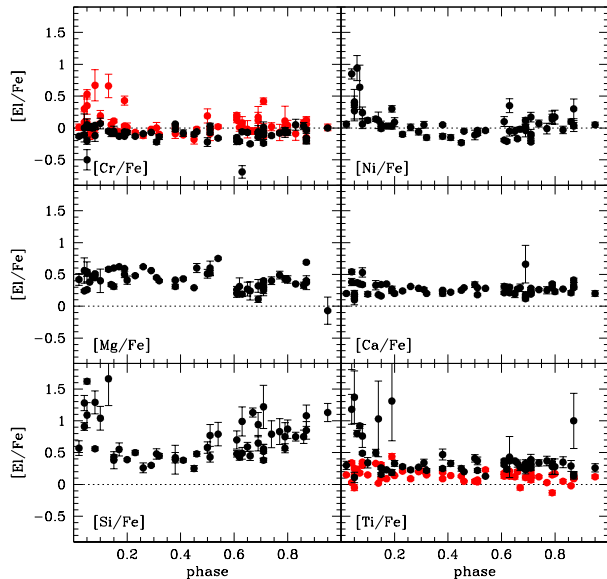


Figure 7. Abundance ratios of single spectra plotted versus phase. Black dots are for neutral species and red dots for ionized species (see text for details), errorbars are the σ of all surviving lines divided by the square root of the number of lines.

who found a very similar result, the offset is likely caused by uncertainties in the $\log gf$ values of Ti I lines, but lacking a clearer explanation, we chose to obtain $[\text{Ti}/\text{Fe}]$ as a weighted average of $[\text{Ti I}/\text{Fe}]$ and $[\text{Ti II}/\text{Fe}]$, as done for Cr.

Once the weighted averages of α -element ratios were computed for each star, we observed that the results were broadly compatible with the typical halo α -enhancement (Figure 8), except for silicon — as said above — with no significant trends with $[\text{Fe}/\text{H}]$. We obtained: $\langle [\text{Mg}/\text{Fe}] \rangle = +0.43 \pm 0.12$ dex, $\langle [\text{Ca}/\text{Fe}] \rangle = +0.27 \pm 0.10$ dex, $\langle [\text{Si}/\text{Fe}] \rangle = +0.73 \pm 0.30$ dex, and $\langle [\text{Ti}/\text{Fe}] \rangle = +0.26 \pm 0.23$ dex. The average α -enhancement is $\langle [\alpha/\text{Fe}] \rangle = +0.31 \pm 0.19$ dex when excluding silicon (when including it, both the enhancement and the error are higher by 0.1 dex).

4.6 Literature comparisons

Five of our program stars were analyzed in the past with high-resolution spectroscopy: TU UMa, VX Her, X Ari, TW Cap, and UY Eri.

TU UMa was observed at phase 0.77 by Clementini et al. (1995) and at phase 0.09 by Butler et al. (1979). Their adopted T_{eff} are fully consistent with the shaded area in Figure 4, covered by the For et al. (2011) analysis, and thus with our adopted value; their gravities are generally higher, more consistent with the Baade-Wesselink results (see Section 4.2 and For et al. 2011); their v_t are well above 3 km/s, i.e., 2–3.5 km/s higher than our value, as expected because of the EW fitting method adopted here (Section 4.3). However, their resulting $[\text{Fe}/\text{H}]$ abundances of -1.05 dex (Butler et al. 1979) and -1.55 dex (Clementini et al. 1995) nicely bracket our value of -1.31 dex, and our determination is compatible with both values, considering their quoted errorbars of 0.1 dex (Clementini et al. 1995) and 0.14 dex (Butler et al. 1979).

VX Her was observed by Clementini et al. (1995) at five phases in the range 0.54–0.69. Their T_{eff} value of 5950 ± 115 K

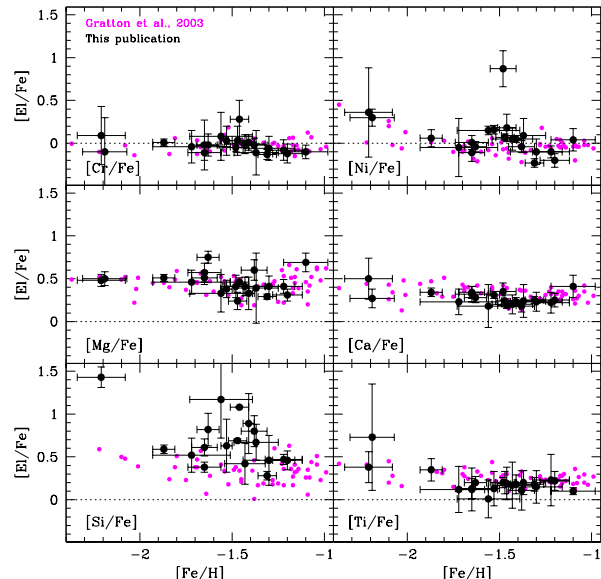


Figure 8. Weighted average abundance ratios for each star with 1σ errors, plotted versus $[\text{Fe}/\text{H}]$ (see text for details). The field stars abundance ratios measured by Gratton et al. (2003) are reported as magenta dots in all panels.

is included in the shaded area in Figure 4, and is thus compatible with our adopted value; their $\log g$ is 2.6 dex, again in line with the Baade-Wesselink determinations; their v_t is 4.5 km/s, thus higher than our determination, as expected. Their resulting $[\text{Fe}/\text{H}] = -1.58$ dex is very close to the one derived here of -1.56 dex.

The comparison with literature data for X Ari is not straightforward. We found three different high-resolution studies: Clementini et al. (1995); Lambert et al. (1996); and Haschke et al. (2012). They obtained $[\text{Fe}/\text{H}]$ of -2.47 , -2.47 , and -2.61 dex, respectively, which are 0.3–0.4 dex lower than our determination. These determinations are only marginally incompatible with the one presented here, given our large combined uncertainty of 0.24 dex, that is mostly due to our large uncertainties in the atmospheric parameters. As a test, we ran again our abundance computations using fixed parameters, more in line with the ones adopted in those studies, i.e., $T_{\text{eff}} = 6300$ K, $\log g = 2.5$ dex and $v_t = 4.5$ km/s: we obtained a much lower $[\text{Fe}/\text{H}] = -2.71$ dex, but at the expense of the ionization and excitation equilibria, and of the flatness of the $[\text{Fe}/\text{H}]$ vs. EW trend²⁰. We thus concluded that our spectrum of X Ari does not allow for such low metallicities and we proceeded to look for additional literature determinations. We found: $[\text{Fe}/\text{H}] = -2.01$ dex with the ΔS method (Suntzeff, Kraft, & Kinman 1994); and $[\text{Fe}/\text{H}] = -1.97$ dex from the Baade-Wesselink method (Blanco 1992). These add to the $[\text{Fe}/\text{H}] = -2.08$ dex by Kinemuchi et al. (2006), although Beers et al. (2000) reports -2.43 dex. Our result of -2.19 dex therefore appears to lie in between two groups of discrepant literature values, and we would weaken the internal con-

²⁰ More in detail, we obtain a slope of -0.013 dex/eV for the $[\text{Fe}/\text{H}]$ vs. excitation potential relation, a slope of -0.16 dex/mÅ for the $[\text{Fe}/\text{H}]$ vs. EW relation, and a difference of -0.18 dex between Fe I and Fe II. With our parameters we obtain instead a slope of 0.0063 dex/eV for the $[\text{Fe}/\text{H}]$ vs. excitation potential relation, a slope of -0.44 dex/mÅ for the $[\text{Fe}/\text{H}]$ vs. EW relation, and a difference of -0.11 dex between Fe I and Fe II.

sistency of our analysis if we adopted significantly different atmospheric parameters.

TW Cap, one of our three Population II Cepheids, was studied by Maas et al. (2007). They do not report the phase of their observations, but they rejected all spectra showing asymmetric line profiles, thus we can assume that their spectra were far from the shock phases. Their parameters were obtained with a method similar to ours, but they differ from our analysis, being: $T_{\text{eff}}=5250$ K, i.e., significantly lower than the typical estimates in this paper and in For et al. (2011); $\log g=0.5$ dex likewise among the lowest estimates we encountered in the literature; $v_t=3.1$ km/s, roughly compatible with the For et al. (2011) typical values, but higher than our typical estimates, and lower than the typical v_t values in older abundance analysis papers quoted so far. Finally, they obtain $[\text{Fe}/\text{H}]=-1.8$ dex, which is formally consistent with our estimate.

UY Eri is another of our Population II Cepheids, also studied by Maas et al. (2007) with high-resolution spectroscopy. They obtain: $T_{\text{eff}}=6000$ K, which is substantially lower than our estimate; $\log g=1.5$ dex, roughly compatible with our estimate, $v_t=2.9$ km/s, higher than our estimate. In this case, their final $[\text{Fe}/\text{H}]=-1.84$ dex does not agree with our derived -1.43 ± 0.20 dex. We thus tried employing the parameters adopted by Maas et al. (2007), even if we do not know at which pulsation phase they were evaluated, and examined the impact on our abundance analysis. As expected, the constancy of $[\text{Fe}/\text{H}]$ versus excitation potential, EW, and wavelength were totally disrupted, together with the ionization balance between Fe I and Fe II, thus proving that our data cannot support parameters much different than the ones adopted here. However, the resulting $[\text{Fe}/\text{H}]$ went substantially down, below -2 dex, showing that the different choice of the parameters is the most likely cause for the different iron abundances.

In conclusion, the presented literature comparisons (see also Section 4.4) generally support the results obtained with our data and method. There are marginal disagreements for X Ari and UY Eri, that can be at least partially explained by the different assumptions on atmospheric parameters, as discussed above.

5 DISCUSSION AND CONCLUSIONS

We have analysed a sample of 21 variable stars — mostly RRab, with one RRC, two BL Her and one W Vir — having high-resolution spectra from both proprietary (UVES and SARG) and archival (UVES, HARPS, FEROS, APO) sets. The data were taken at random phases and as a consequence several spectra were obtained outside optimal phases, and a few spectra very close to the shock phases.

We performed a classical EW-based abundance analysis with static stellar atmospheric models and obtained consistent metallicities (Section 4.4) and abundance ratios (Sections 4.5) — within roughly 0.15 dex — regardless of the phase, even for those spectra very close to the shock phases. It is interesting to note that the W Vir variable (TW Cap) and the two BL Her variables (UY Eri and V716 Oph) behave exactly like RRab at all phases, and thus appear virtually indistinguishable, from the spectroscopic analysis point of view, at least in the sampled phases. While this result is not surprising, given that the physical mechanism responsible for the pulsation is the same and the stellar parameters are quite similar, this is the first time a sample comprising both RR Lyrae (RRab and RRC) and Population II Cepheids is analyzed homogeneously.

Comparisons with the Beers et al. (2000) and Kinemuchi et al. (2006) samples, based on $[\text{Fe}/\text{H}]$ calibrations for RR Lyrae, showed

a rather satisfactory scatter of roughly 0.20 dex, with no significant offset or phase trend (Section 4.4), and comparisons with high-resolution studies (Section 4.6) generally supported our abundance analysis. Iron-peak elements were overall solar, again with no trends with phase and a moderate scatter of roughly 0.15 dex. An average $[\alpha/\text{Fe}]=+0.31\pm0.19$ dex was found over the entire sample, based on Mg, Ca, Ti I, and Ti II. The expected problematic element was silicon, which was discussed in detail in the literature (see For et al. 2011, for references): it was rather difficult to find reliable lines, producing relatively small scatter and a $[\text{Si}/\text{Fe}]$ abundance independent from the phase. Also, a small but systematic ionization imbalance of $\langle\Delta[\text{Cr}/\text{Fe}]\rangle=-0.11\pm0.11$ dex and $\langle\Delta[\text{Ti}/\text{Fe}]\rangle=+0.18\pm0.10$ dex was observed, as reported by previous authors, and most probably caused by uncertainties in the $\log gf$ values.

Our spectroscopically derived atmospheric parameters are also broadly consistent with the ones expected from template curves (Sections 4.1, 4.2, and 4.3) for RRab and Population II Cepheids, while for U Com, the only RRC in our sample, template curves give a too high T_{eff} that was not reported in previous work (see for example Lambert et al. 1996; Govea et al. 2014). Also, the atmospheric parameters found in the present analysis were broadly consistent with the ones found in the similar analysis performed by For et al. (2011), with scatters around the expected values of roughly ± 300 K for T_{eff} , ± 0.3 dex for $\log g$, and ± 0.4 km/s for v_t .

In summary, a classical EW-based abundance analysis on high-resolution ($R\geq 30\,000$), high S/N spectra ($S/N\geq 30$) is appropriate to study RR Lyrae spectra at all phases, with a possible danger only in the range $0 \lesssim \phi \lesssim 0.15$ (where the abundance ratios could be overestimated, depending on the species), and with relatively long exposure times (up to 45 min), provided absorption lines are carefully selected and as long as an error of about 0.10–0.15 dex is considered acceptable.

ACKNOWLEDGMENTS

We would like to thank E. Bernard for useful discussions on the $[\text{Fe}/\text{H}]$ calibrations of RR Lyrae based on pulsation properties, and G. Fiorentino for help on the Population II Cepheids properties and classification. We warmly thank C. Sneden, who was the referee of this paper, for his insightful comments. N. Britavskiy acknowledges the support of the European Commission Erasmus Mundus LOT 7 programme and warmly thanks the INAF–Bologna Observatory, where most of this work was carried out, for the hospitality during the grant stay. D. Romano acknowledges financial support from PRIN MIUR 2010–2011, project “The chemical and dynamical evolution of the Milky Way and Local Group galaxies”, prot. 2010LYSN2T. This publication makes use of data products from the Two Micron All Sky Survey, which is a joint project of the University of Massachusetts and the Infrared Processing and Analysis Center/California Institute of Technology, funded by the National Aeronautics and Space Administration and the National Science Foundation. This publication makes use of the data from the Northern Sky Variability Survey (NSVS) created jointly by the Los Alamos National Laboratory and University of Michigan. The NSVS was funded by the Department of Energy, the National Aeronautics and Space Administration, and the National Science Foundation. This research made use of the products of the Cosmic-Lab project funded by the European Research Council. In this work we made extensive use of the NASA ADS abstract service, of the Stras-

bourg CDS database, and of the atomic data compiled in the VALD data base.

REFERENCES

- Alcock C., et al., 2000, *ApJ*, 542, 257
- Allende Prieto C., García López R. J., Lambert D. L., Gustafsson B., 1999, *ApJ*, 527, 879
- Alonso A., Arribas S., Martínez-Roger C., 1999, *A&AS*, 140, 261
- Bailey, S., *AnHar* 38, 1
- Ballester P., Modigliani A., Boitquin O., Cristiani S., Hanuschik R., Kaufer A., Wolf S., 2000, *The Messenger*, 101, 31
- Beers T. C., Rossi S., Norris J. E., Ryan S. G., Shefler T., 1999, *AJ*, 117, 981
- Beers T. C., Chiba M., Yoshii Y., Platais I., Hanson R. B., Fuchs B., Rossi S., 2000, *AJ*, 119, 2866
- Bekki K., Freeman K. C., 2003, *MNRAS*, 346, L11
- Benedict G. F., et al., 2011, *AJ*, 142, 187
- Blanco V. M., 1992, *AJ*, 104, 734
- Blazhko S., 1907, *Astron. Nachr.*, 175, 325
- Bono G., Caputo F., Di Criscienzo M., 2007, *A&A*, 476, 779
- Butler D., Carbon D., Kraft R. P., 1976, *ApJ*, 210, 120
- Butler D., Kraft R. P., Kinman T. D., 1979, *AJ*, 84, 993
- Cacciari C., Clementini G., 2003, in Alloin D., Gieren W., eds, *Lecture Notes in Physics*, Vol. 635, *Stellar Candles for the Extragalactic Distance Scale*. Springer, Berlin, p. 105
- Cacciari C., Clementini G., Prevot L., Lindgren H., Lolli M., Oculi L., 1987, *A&AS*, 69, 135
- Cantat-Gaudin T., et al., 2014, *A&A*, 562, A10
- Castelli F., Kurucz R. L., 2003, in Piskunov N., Weiss W. W., Gray D. F., eds, *Proc. IAU Symp. 210, Modelling of Stellar Atmospheres*. Astron. Soc. Pac., San Francisco, p. A20
- Catelan M., 1992, *A&A*, 261, 457
- Chadid M., Vernin J., Gillet D., 2008, *A&A*, 491, 537
- Chadid M., Preston G. W., 2013, *MNRAS*, 434, 552
- Clementini G., Cacciari C., Lindgren H., 1990, *A&AS*, 85, 865
- Clementini G., Carretta E., Gratton R., Merighi R., Mould J. R., McCarthy J. K., 1995, *AJ*, 110, 2319
- Clementini G., Gratton R. G., Bragaglia A., Ripepi V., Martinez Fiorenzano A. F., Held E. V., Carretta E., 2005, *ApJ*, 630, L145
- Clementini G., Merighi R., Pasquini L., Cacciari C., Gouiffes C., 1994, *MNRAS*, 267, 83
- Dekker H., D'Odorico S., Kaufer A., Delabre B., Kotzlwski H., 2000, *Proc. SPIE*, 4008, 534
- Dinescu D. I., 2002, in van Leeuwen F., Hughes J. D., Piotto G., eds, *ASP Conf. Ser. Vol. 265, Omega Centauri: A Unique Window into Astrophysics*. Astron. Soc. Pac., San Francisco, p. 365
- D'Odorico S., 2000, *The Messenger*, 99, 2
- Drake A. J., Catelan M., Djorgovski S. G., et al., 2013, *ApJ*, 765, 154
- Fernley J., Barnes T. G., 1997, *A&AS*, 125, 313
- Fernley J. A., Lynas-Gray A. E., Skillen I., Jameson R. F., Marang F., Kilkenny D., Longmore A. J., 1989, *MNRAS*, 236, 447
- Fokin A. B., 1992, *MNRAS*, 256, 26
- Fokin A. B., Gillet D., Chadid M., 1999, *A&A*, 344, 930
- For B.-Q., Sneden C., 2010, *AJ*, 140, 1694
- For B.-Q., Sneden C., Preston G., 2011, *ApJS*, 197, 29
- Fossati L., Kolenberg K., Shulyak D. V., Elmasli A., Tsymbal V., Barnes T. G., Guggenberger E., Kochukhov O., 2014, *arXiv:1410.4380*
- Fuhr J. R., Martin G. A., Wiese W. L., 1988, *JPCRD*, 17, 1
- Gillet D., Crowe R. A., 1988, *A&A*, 199, 242
- Gillet D., Burki G., Crowe R. A., 1989, *A&A*, 225, 445
- Gratton R. G., et al., 2001, *Exp. Astron.*, 12, 107
- Gratton R. G., Carretta E., Desidera S., Lucatello S., Mazzei P., Barbieri M., 2003, *A&A*, 406, 131
- Grevesse N., Sauval A. J., 1998, *Space Sci. Rev.*, 85, 161
- Govea J., Gomez T., Preston G. W., Sneden C., 2014, *ApJ*, 782, 59
- Haschke R., Grebel E. K., Frebel A., Duffau S., Hansen C. J., Koch A., 2012, *AJ*, 144, 88
- Hill S. J., 1972, *ApJ*, 178, 793
- Høg E., et al., 2000, *A&A*, 355, L27
- Jerzykiewicz M., Wenzel W., 1977, *Acta Astron.*, 27, 35
- Jones R. V., Carney B. W., Fulbright J. P., 1996, *PASP*, 108, 877
- Jurcsik J., Kovacs G., 1996, *A&A*, 312, 111
- Jurcsik J., Sódor Á., Szeidl B., et al., 2009, *MNRAS*, 400, 1006
- Kinemuchi K., Smith H. A., Woźniak P. R., McKay T. A., ROTSE Collaboration, 2006, *AJ*, 132, 1202
- Kinman T. D., Aoki W., Beers T. C., Brown W. R., 2012, *ApJ*, 755, L18
- Kolenberg K., Fossati L., Shulyak D., Pikall H., Barnes T. G., Kochukov O., Tsymbal V., 2010, *A&A*, 519, A64
- Kupka F. G., Ryabchikova T. A., Piskunov N. E., Stempels H. C., Weiss W. W., 2000, *Balt. Astron.*, 9, 590
- Kurucz R. L., 2005, *Mem. Soc. Astron. Italiana Suppl.*, 8, 14
- Lambert D. L., Heath J. E., Lemke M., Drake J., 1996, *ApJS*, 103, 183
- Le Borgne J. F., et al., 2007, *A&A*, 476, 307
- Lebre A., 1993, in Nemec J. M., Matthews J. M., eds, *Proc. IAU Colloq. 139, New Perspectives on Stellar Pulsation and Pulsating Variable Stars*. Cambridge Univ. Press, Cambridge, p. 376
- Liu T., Janes K. A., 1989, *ApJS*, 69, 593
- Liu T., Janes K. A., 1990, *ApJ*, 354, 273
- Maas T., Giridhar S., Lambert D. L., 2007, *ApJ*, 666, 378
- Maintz G., 2005, *A&A*, 442, 381
- Majewski S. R., Nidever D. L., Smith V. V., Damke G. J., Kunkel W. E., Patterson R. J., Bizyaev D., García Pérez A. E., 2012, *ApJ*, 747, L37
- Meléndez J., Barbuy B., 2009, *A&A*, 497, 611
- Meyer R., 2006, *OEJV*, 21, 1
- Meza A., Navarro J. F., Abadi M. G., Steinmetz M., 2005, *MNRAS*, 339, 93
- Mizutani A., Chiba M., Sakamoto T., 2003, *ApJ*, 589, L89
- Moore C. E., Minnaert M. G. J., Houtgast J., 1966, *The Solar Spectrum 2935 Å to 8770 Å*, NBS Monogr., No. 61
- Moretti M. I., Clementini G., Muraveva T., et al., 2014, *MNRAS*, 437, 2702
- Mucciarelli A., Pancino E., Lovisi L., Ferraro F. R., Lapenna E., 2013, *ApJ*, 766, 78
- Oke J. B., 1966, *ApJ*, 145, 468
- Pickering J. C., Thorne A. P., Perez R., 2001, *ApJS*, 132, 403
- Pojmanski G., 1997, *AcA*, 47, 467
- Preston G. W., 1964, *ARA&A*, 2, 23
- Preston G. W., 2011, *AJ*, 141, 6
- Preston G. W., Paczynski B., 1964, *ApJ*, 140, 181
- Preston G. W., Smak J., Paczynski B., 1965, *ApJS*, 12, 99
- Preston G. W., Thompson I. B., Sneden C., Stachowski G., Shectman S. A., 2006, *AJ*, 132, 1714
- Preston G. W., Chadid M., 2013, *EAS*, 63, 35
- Samus N. N., Kazarovets E. V., Kireeva N. N., Pastukhova E. N., Durlevich O. V., 2010, *Odessa Astron. Publ.*, 23, 102
- Sandage A., 1993, *AJ*, 106, 687

- Sandage A., 2004, *AJ*, 128, 858
- Sanford R. F., 1949, *PASP*, 61, 135
- Sbordone L., Bonifacio P., Castelli F., Kurucz R. L., 2004, *Mem. Soc. Astron. Italiana Suppl.*, 5, 93
- Schlafly E. F., Finkbeiner D. P., 2011, *ApJ*, 737, 103
- Sesar B., Ivezić Ž, Grammer S. H., et al., 2010, *ApJ*, 708, 717
- Sesar B., Grillmair C. J., Cohen J. G., et al., 2013, *ApJ*, 776, 26
- Shi J. R., Gehren T., Mashonkina L., Zhao G., 2009, *A&A*, 503, 533
- Smith H. A., 1995, *RR Lyrae Stars*. Cambridge Univ. Press, Cambridge
- Skrutskie M. F., et al., 2006, *AJ*, 131, 1163
- Sobeck J. S., Lawler J. E., Sneden C., 2007, *ApJ*, 667, 1267
- Soszyński I. et al., 2008, *Acta Astron.*, 58, 293
- Stetson P. B., Pancino E., 2008, *PASP*, 120, 1332
- Struve O., 1947, *PASP*, 59, 192
- Suntzeff N. B., Kraft R. P., Kinman T. D., 1994, *ApJS*, 93, 271
- Tsuchiya T., Korchagin V. I., Dinescu D. I., 2004, *MNRAS*, 350, 1141
- Tsymbal V. V. 1996, in Adelman S. J., Kupka F., Weiss W. W., eds, *ASP Conf. Ser. Vol. 108, Model Atmospheres and Spectrum Synthesis*. Astron. Soc. Pac., San Francisco, p. 198
- van Leeuwen F., 2007, *A&A*, 474, 653
- Vivas A. K., Jaffé Y. L., Zinn R., Winnick R., Duffau S., Mateu C., 2008, *AJ*, 136, 1645
- Wallerstein G., Gomez T., Huang W., 2012, *Ap&SS*, 341, 89
- Wiese L. M., Fedchak J. A., Lawler J. E., 2001, *ApJ*, 547, 1178
- Woźniak P. R., et al., 2004, *AJ*, 127, 2436
- Wylie-de Boer E., Freeman K., Williams M., 2010, *AJ*, 139, 636
- Zinn R., West M. J., 1984, *ApJS*, 55, 45